Evaluation of IL-1 blockade as a host-directed therapy for tuberculosis in mice and macaques

Caylin G. Winchell[1], Bibhuti B. Mishra [2,3], Jia Yao Phuah[2], Mohd Saqib[3], Samantha J. Nelson[2], Pauline Maiello[1], Chelsea M. Causgrove[1], Cassaundra L. Ameel[1], Brianne Stein[1], H. Jacob Borish[1], Alexander G. White[1], Edwin C. Klein[4], Matthew D. Zimmerman[5¥], Véronique Dartois[5¥], Philana Ling Lin[6], Christopher M. Sassetti[2], JoAnne L. Flynn[1*]

[1]Department of Microbiology and Molecular Genetics, University of Pittsburgh School of Medicine, Pittsburgh, Pennsylvania, USA

[2]Department of Microbiology and Physiological Systems, University of Massachusetts Medical School, Worcester, Massachusetts, USA

[3]Department of Immunology and Microbial Disease, Albany Medical College, Albany, New York, USA

[4]Division of Laboratory Animal Research, University of Pittsburgh, Pittsburgh Pennsylvania, USA

[5]Public Health Research Institute, New Jersey Medical School, Rutgers, The State University of New Jersey, Newark, NJ, USA

[6]Department of Pediatrics, UPMC Children's Hospital of the University of Pittsburgh, Pittsburgh, Pennsylvania, USA

[¥] Present address: Center for Discovery and Innovation, Hackensack Meridian Health, Nutley, NJ, USA

* Corresponding author

Email: joanne@pitt.edu

Abstract

In 2017, there were over 550,000 estimated new cases of multi-drug/rifampicin resistant tuberculosis (MDR/RR-TB), emphasizing a need for new treatment strategies. Linezolid (LZD) is a potent antibiotic for antibiotic-resistant Gram-positive infections and is an effective treatment for TB. However, extended LZD use can lead to LZD-associated host toxicities, most commonly bone marrow suppression. LZD toxicities may be mediated by IL-1, a pathway important for early immunity during *M. tuberculosis* infection that later contributes to pathology. We hypothesized LZD efficacy could be enhanced by modulation of IL-1 pathway to reduce BM toxicity and TB associated-inflammation. We used two animal models of TB to test our hypothesis, mice and cynomolgus macaques. Antagonizing IL-1 in chronically-infected mice reduced lung neutrophil numbers and partially restored the erythroid progenitor populations that are depleted by LZD. In macaques, we found no conclusive evidence of BM suppression associated with LZD, indicating our treatment time may have been short enough to avoid the toxicities observed in humans. Though treatment was only 1 month, the majority of granulomas were sterilized with reduced inflammation (assessed by PET/CT) in animals treated with both LZD and IL-1 receptor antagonist (IL-1Rn). However, overall lung inflammation was significantly reduced in macaques treated with both IL-1Rn and LZD, compared to LZD alone. Importantly, IL-1Rn administration did not noticeably impair the host response against Mtb or LZD efficacy in either animal model. Together, our data support that inhibition of IL-1 in combination with LZD has potential to be an effective HDT for TB.

Author summary

Host-directed therapies (HDTs) are a potential option in combating drug resistant TB as they can circumvent bacterial drug-resistance by targeting host responses rather than the pathogen. Here we designed an HDT to target the IL-1 pathway, an inflammatory immune

61 response that is both critical and detrimental to TB disease outcome. We combined IL-1Rn, an
62 IL-1R antagonist, with linezolid (LZD) which is an effective antibiotic for drug-resistant M.
63 tuberculosis. Extended treatment causes severe host-toxicities that might be mediated in part
64 by the IL-1 pathway. Our goals were to enhance LZD efficacy by negating LZD-host toxicities
65 and to reduce adverse inflammation caused by TB. In mice, IL-1Rn effectively reduced
66 inflammatory signatures associated with TB and reversed linezolid-induced bone marrow
67 suppression, the most common toxicity. In cynomolgus macaques, inflammation, as assessed
68 by PET/CT, was reduced by the combination of IL-1Rn and LZD therapy, compared to LZD
69 alone. In contrast to mice, we did not observe bone marrow suppression in macaques,
70 highlighting the importance of both models when assessing prospective therapies. These data
71 show the potential of IL-1Rn as a therapy for TB and support LZD as an effective antibiotic
72 against drug-resistant TB.
73

74 Introduction

75 Tuberculosis (TB) remains the top cause of death by a single infectious agent, with an
76 estimated 10 million new active TB cases and 1.3 million deaths in 2017 alone (1). Antibiotic
77 treatment regimens are long and multi-drug resistant (MDR) and extensive-drug resistant (XDR)
78 *Mycobacterium tuberculosis* (Mtb) strains have emerged, complicating treatment. Even those
79 patients that are cured of the infection can suffer permanent deficits in lung function that result
80 from inflammation and fibrosis (2). Host-directed therapies (HDTs) have been proposed as a
81 potential option for improving therapy. Depending on the strategy, HDTs could enhance
82 antimicrobial immune responses and shorten therapy, or inhibit pathological inflammation (3).
83 Since HDT would be used as part of a multi-drug regimen, targeting mechanisms that increase
84 drug exposure or decrease toxicity could also be envisioned. While some HDT strategies hold
85 promise, very few have been rigorously tested in pre-clinical models (4).

86

87 Interleukin-1 (IL-1) has been implicated in TB disease and inflammation, making it a possible
88 target of HDT. This cytokine plays an important yet complicated role in TB disease progression.
89 The susceptibility of mice lacking critical mediators of IL-1 signaling indicates that some initial
90 production of IL-1β upon Mtb infection is essential for priming downstream immune responses
91 necessary for disease control (5-8). In contrast, IL-1 is also responsible for the accumulation of
92 disease-promoting neutrophils in chronically-infected susceptible mice, and genetic variants that
93 result in higher IL-1β production are associated with increased disease severity and neutrophil
94 accumulation in humans (9-11). Given that HDT is designed to be administered to chronically-
95 infected patients during treatment, when persistent IL-1 production appears to play a more
96 pathological role, it could be beneficial to block the inflammation and disease promoting
97 activities of this cytokine.

98

99 IL-1 may also play a role in the toxicity of linezolid (LZD), an increasingly important antibiotic for
100 the treatment of drug-resistant TB, highlighted by its recent inclusion in a newly approved
101 therapy for MDR-TB (12). While LZD has shown efficacy against XDR and MDR TB, its wide-
102 spread use has been limited by severe host toxicities that occur after more than 4 weeks of
103 treatment (13, 14). Over the 6-20 month treatment course necessary to treat resistant TB, both
104 reversible bone marrow suppression and irreversible neuropathies are common (15). LZD-
105 associated toxicities are generally attributed to the inhibition of mitochondrial translation and
106 LZD-mediated bone marrow suppression is promoted by the subsequent mitochondrial damage.
107 This damage acts on the NOD-like receptor family, pyrin domain containing 3 (NLRP3) protein
108 that has been shown to be necessary for LZD-mediated bone marrow suppression in mice (16).
109 NLRP3, in conjunction with caspase-1 and ASC, forms an inflammasome complex, which
110 cleaves a number of substrates resulting in cell death and/or the release of active of IL-1β.

111 While the importance of NLRP3 in bone marrow suppression is clear, the relative roles of
112 inflammasome activation and IL-1 signaling remain uncertain.
113
114 Based on these observations, inhibiting the IL-1 pathway by HDT could serve two purposes:
115 first, to alleviate LZD-associated host toxicity, and second, to reduce the pathology associated
116 with the IL-1 pathway during TB disease. Due to the pro-inflammatory nature of the IL-1
117 pathway, strict regulatory mechanisms exist within the host to quell this pathway. IL-1 receptor
118 antagonist (IL-1Rn) is a protein produced constitutively at low levels that can increase in
119 response to a variety of cytokine signals. IL-1Rn serves as a decoy ligand for the IL-1R1,
120 blocking signal transduction and subduing activation of subsequent pro-inflammatory pathways
121 (17). Anakinra is an FDA-approved recombinant IL-1Rn that is used to treat rheumatoid
122 arthritis. As there are no FDA approved drugs to inhibit inflammasome activation, inhibition of
123 the IL-1 pathway with biologics, such as Anakinra, is the only currently feasible strategy to
124 modulate this pathway (18).
125
126 We hypothesized that the combination of Anakinra (herein referred to as IL-1Rn) with LZD for
127 treatment of active TB disease would reduce LZD-associated toxicities and host inflammation
128 resulting in a more efficacious therapy. To test this concept, we employed two established TB
129 animal models to assess differing aspects of host responses to LZD and IL-1Rn. We used
130 multiple strains of mice to model distinct disease states and dissect the relative importance of
131 the inflammasome and IL-1 signaling in HDT efficacy. As a translational model, we used
132 cynomolgus macaques in combination with [^{18}F] FDG PET/CT serial imaging to track TB
133 disease progression, including inflammation, before and during drug regimens (19).
134 Cynomolgus macaques present with a similar spectrum of Mtb infection as humans, with
135 pathology, including granuloma structure and diversity, that recapitulates human TB (20-22).
136 Together, our data further verify LZD as an efficacious antibiotic in both mice and macaques

137 and indicate that addition of IL-1Rn may accelerate the resolution of inflammation and partially
138 alleviate LZD-mediated BM suppression.
139

140 ## Results

141 **IL-1 receptor blockade reduces inflammation in mouse models of TB disease.**

142 Given the complex role played by IL-1 during TB, we initially sought to determine the effect of
143 inhibiting this cytokine during established TB disease in mice. These studies compared two IL-1
144 antagonists, a blocking antibody to the murine IL-1 receptor (αIL-1R1) and the human IL-1
145 receptor antagonist, Anakinra (IL-1Rn), each delivered between days 14 and 28 post infection.
146 Two mouse strains were employed to assess the effects of these treatments in animals with
147 different amounts of IL-1 activity. In relatively resistant C57BL/6 animals, mature IL-1
148 production is controlled during chronic disease, whereas unregulated IL-1 drives inflammatory
149 disease in Mtb-infected *Nos2*$^{-/-}$ mice (9, 10).
150

151 While the human IL-1Rn had little effect in these models, the αIL-1R1 treatment significantly
152 reduced PMN numbers in the lungs of both resistant and susceptible mouse strains, and
153 reversed the weight loss observed in *Nos2*$^{-/-}$ mice (Fig. 1A-B). While neither regimen
154 significantly altered the lung bacterial burden, both IL-1Rn and αIL-1R1 treatment reduced
155 bacterial burden in the spleens of *Nos2*$^{-/-}$ mice (Fig. 1C-D). This generally beneficial effect of
156 αIL-1R1 treatment was consistent with qualitatively improved histopathological disease (Fig.
157 1E). By no metric did αIL-1R1 treatment exacerbate established disease in either mouse strain.
158

159 **IL-1 blockade alleviates lung inflammation and hematopoietic suppression during**
160 **LZD treatment in mice.**

161 The IL-1R1 blocking antibody αIL-1R1 was next tested in combination with LZD to determine
162 whether the efficacy or toxicity of the antibiotic was altered. C3HeB/FeJ mice, which are
163 relatively susceptible to Mtb and develop histopathological lesions that more closely resemble
164 human disease, were used for these studies. Mice with established disease were treated
165 between days 28 and 46 post-infection with vehicle alone, LZD, αIL-1R1 or a combination of the
166 two. As previously reported, LZD was effective in this model, reducing lung neutrophil numbers,
167 bacterial burden and weight loss (Fig. 2 A-D) (23). The addition of αIL-1R1 to this regimen
168 further reduced lung neutrophil numbers, and did not significantly alter the antimicrobial activity
169 of LZD. As IL-1β production in response to both Mtb infection and LZD treatment depends
170 largely on the NLRP3 inflammasome, we also investigated a regimen in which LZD and a small
171 molecule NLRP3 inhibitor (MCC950) was administered between days 56 and 77 post-infection.
172 As observed with αIL-1R1, the addition of MCC950 reduced PMN numbers in the lung, relative
173 to LZD alone, and did not significantly alter the rate of bacterial killing (Fig. 2 E-G). Using a
174 more rapid treatment protocol and C57BL/6 mice with genetic deficiencies in Caspase 1 or
175 NLRP3, we confirmed that the antimicrobial activity of LZD was unaffected by inflammasome
176 activation (Supplementary Fig. 1). Mice were treated between days 14 and 28 post-infection
177 and the effect of LZD on bacterial burden and lung neutrophil number was at least as large in
178 the knockout animals as the wild type controls.
179
180 Hematopoietic suppression was assayed in bone marrow and spleens of C3HeB/FeJ mice.
181 Both organs are significant sites for hematopoiesis in small animals, in which the bone marrow
182 has insufficient capacity, particularly when the requirement for blood cells increases. Using flow
183 cytometry, erythroid progenitors can be divided into a progression of precursors; pro-erythrocyte
184 (ProE), EryA, EryB, and EryC (Fig. 3A). These populations were quantified in each tissue of
185 Mtb-infected animals treated with LZD and/or αIL-1R1. In both bone marrow and spleen, LZD

186 had a profound effect, nearly eliminating early erythroid progenitors of the ProE, EryA and EryB
187 classes (Fig. 3B-E). Simultaneous treatment with αIL-1R1 largely reversed the effect of LZD in
188 the spleen, restoring these immature precursors to approximately half of their untreated levels.
189 While αIL-1R1 also significantly increased the number of erythroid precursors in the BM, the
190 suppression of LZD toxicity was less pronounced at this site.
191
192 In sum, studies in the mouse model indicated that the addition of αIL-1R1 to an LZD regimen
193 could reduce the number of lungs PMN and ameliorate hematopoietic toxicity, while not
194 compromising antimicrobial activity. These observations justified further studies in a non-human
195 primate model.
196
197 **Changes in TB disease in macaques treated with LZD and HDT by PET/CT**
198 Previously we published the efficacy and pharmacokinetics of LZD in cynomolgus macaques
199 treated for 8 weeks with a single daily dose of 30 mg/kg (14). To adhere to FDA guidelines for
200 LZD administration at the time we initiated this study, and reproduce clinical exposure at 600 mg
201 twice daily (b.i.d.), we shortened treatment duration to 4 weeks and increased the dosing
202 frequency to 30 mg/kg b.i.d. Dose finding studies were carried out in uninfected cynomolgus
203 macaques to ensure that adequate drug concentrations similar to those achieved in patients at
204 600 mg b.i.d. were reached in the blood (Supplementary Fig. 2A).
205
206 To assess this HDT/LZD regimen, we infected 10 cynomolgus macaques with Mtb strain
207 Erdman (12 CFU via bronchoscope) and monitored development of active TB disease (~3-5
208 months) (Supplementary Table 1 and Supplementary Fig. 2B). The macaques were then
209 randomized to a 4-week drug regimen of LZD (n=5) or LZD+IL-1Rn (n=5) (Supplementary Fig.
210 2B). One advantage of this model is the ability to track disease progression throughout infection

211 and treatment using serial ^{18}F-FDG PET CT scans (14, 24). Lung inflammation was quantified
212 by total FDG activity in the lungs before and during treatment (Fig. 4A-B and Supplementary
213 Table 1)(19). In LZD treated macaques, there was no significant decrease in total lung FDG
214 activity after 4 weeks (p=0.2876), although there was a trend for an initial reduction in
215 inflammation after 2 weeks of treatment (p=0.0857)(Fig. 4B). In contrast, LZD+IL-1Rn treatment
216 resulted in a significant reduction in total lung FDG activity after 2 and 4 weeks (p=0.0242,
217 p=0.0237 respectively). We assessed changes in granulomas during treatment by measuring
218 physical size (CT) and metabolic activity (measured as the standard uptake value of FDG per
219 granuloma, SUVR) (Fig. 4C-D)(19). During treatment, the majority of granulomas decreased in
220 size with no differences between LZD and LZD+IL1-Rn treated animals. However, granuloma
221 metabolic activity (SUVR) was significantly reduced in LZD+IL-1Rn treated macaques
222 compared to those treated with LZD alone for all granulomas. These data indicate that blocking
223 of IL-1R in combination with LZD reduces inflammation in whole lungs and individual
224 granulomas more effectively than LZD treatment alone.
225

226 **Supplementary Table 1. List of macaques for study and PET/hot values**

227

Supplemental Table 1 - Macaque Study Data												
HDT Study												
NHP	Age (yr)	Gender	Infection Dose	Treatment Group	DPI at Treatment Start	Days of Treatment	DPI at Necropsy	Necropsy Score	Total CFU	PreTx PEThot	2wk PEThot	4wk PEThot
29716	5.9	F	12 CFU	LZD	117	28	145	24	61839	526777.88	58333.57	35664.45
29816	7.1	F	12 CFU	LZD	110	28	138	45	4445	11003.65	1309.29	531.02
30016	7	F	12 CFU	LZD	103	29	132	31	1413	85068.79	123759.67	28665.24
30216	7.1	F	12 CFU	LZD	138	31	169	32	1090	2113.02	401.05	3884.92
30316	7.1	F	12 CFU	LZD	117	30	147	37	8005	1453.44	562.79	1828.43
18816	10.9	M	12 CFU	LZD+IL-1Rn	117	30	147	26	505	3236.21	673.86	1520.78
19116	7.2	M	12 CFU	LZD+IL-1Rn	117	28	145	25	330	3304.52	1469.77	1562.60
19416	9.9	M	12 CFU	LZD+IL-1Rn	138	30	168	10	727	872.50	73.54	73.30
20416	8.2	M	12 CFU	LZD+IL-1Rn	110	31	141	28	1260	26957.57	10456.67	2802.92
30116	6.4	F	12 CFU	LZD+IL-1Rn	103	31	134	67	20905	110837.75	48461.60	7609.82
Historical Controls*												
NHP	Age (yr)	Gender	Infection Dose	DPI at Necropsy	Necropsy Score	Total CFU						
18214	8.3	M	39 CFU	84	50	2935647						
18314	8.3	M	39 CFU	91	84	1319857						
1514	6.2	M	38 CFU	118	56	112433						
PET/CT data previously reported in PMID: 28592427												

228 Provided are details regarding macaques utilized for this study. DPI = days post infection.
229

230 **Addition of IL-1Rn does not significantly reduce bacterial burden**

231 While IL-1Rn should not have direct bactericidal activity, this agent could still influence the
232 expression of anti-bacterial immunity. This effect could be beneficial if immune responses are
233 enhanced, or detrimental if IL-1 is necessary for host killing of bacteria. Therefore, we
234 performed comprehensive bacterial burden analysis at necropsy, by identifying the majority of
235 granulomas and other TB pathologies on PET CT scans, obtaining each individually at necropsy
236 and culturing all lesions, thoracic lymph nodes, and uninvolved lung tissue separately, as well
237 as extrapulmonary lesions, as previously described (20). Total thoracic CFU (lung + lymph
238 nodes) was not significantly different between LZD and LZD + IL-1Rn macaques ($p = 0.1508$)
239 (Fig. 5A), with similar frequencies of sterilized granulomas (LZD = 68.42%, LZD+IL-1Rn =
240 72.22%). In the current study, we did not have untreated control macaques, so we provide total
241 thoracic CFU for 3 similarly infected historical controls (untreated) for reference; these data
242 were excluded from statistical analyses. This supports that high dose LZD as a single drug is
243 effective at killing bacteria even in a short (4 week) regimen. Bacterial burden in CFU+ thoracic
244 lymph nodes was similar between the groups though trended towards lower CFU in LZD+IL-
245 1Rn treated macaques ($p=0.0965$) (Fig 5B). We previously reported that a 2-month lower dose
246 regimen of LZD could reduce bacterial burden compared to untreated controls, with ~80%
247 sterilized granulomas (14). Since the bacterial burden in macaques with active TB can vary
248 substantially, we estimated the pre-treatment total thoracic CFU from the total lung FDG by PET
249 CT as previously described (20), and compared the actual bacterial burden post-treatment
250 against the estimated pre-treatment value. All macaques, regardless of treatment group, had
251 lower total thoracic CFU at necropsy compared to the estimated total thoracic CFU prior to
252 treatment initiation (Fig. 5C). Our data indicate that while IL-1Rn did not significantly enhance
253 bacterial killing, it did not impair LZD-mediated bacterial clearance.
254

255 **Lack of LZD-induced bone marrow suppression in macaques**

256 In humans, LZD is associated with host toxicities during extended treatment periods of > 4
257 weeks (25). To determine whether bone marrow suppression occurred during the 4-week high
258 dose LZD therapy and whether IL-1Rn could modulate observable host toxicities, we isolated
259 bone marrow at necropsy from the sternum of each macaque and assessed erythropoietic
260 progenitor populations and mitochondrial function by flow cytometry (Fig. 6A). During
261 homeostatic erythropoiesis, a 1:8 ratio is maintained between ProE and EryC populations,
262 which can be used to indicate disruption to erythropoiesis. There was no significant difference
263 in ProE:EryC ratios between the treatment groups or compared to untreated macaques with Mtb
264 infection (Fig. 6B). However, none of the macaque groups had a homeostatic ratio regardless
265 of treatment. These data indicate that Mtb infection or TB disease alone may disrupt bone
266 marrow homeostasis. To determine whether LZD was affecting bone marrow mitochondrial
267 function, we stained cells with MitoTracker™ Red CMXRos that only stains mitochondria with
268 active membrane potential, indicating function of those organelles (Fig. 6B). Regardless of
269 treatment, the MitoTracker MFI remained similar, indicating that mitochondrial function is the
270 same among groups. To confirm our observations, a pathologist evaluated bone marrow tissue
271 sections and found no observable differences between TB only, LZD and LZD+IL-1Rn groups in
272 terms of cellularity (myeloid:erythroid ratios) or abnormalities (Fig. 6C). While we could not
273 consistently identify progenitor populations in blood or spleen, we performed complete blood
274 counts (CBCs) during treatment to identify signs of bone marrow suppression (i.e., anemia,
275 thrombocytopenia). There were no differences between LZD and LZD+IL-1Rn treatments
276 (Supplementary Fig. 3). In conclusion, 4 weeks of LZD was not sufficient to induce observable
277 bone marrow suppression in cynomolgus macaques and blocking of IL-1R did not alter bone
278 marrow status during LZD treatment of TB.
279
280 **Reduction in inflammatory signatures in the lung after HDT**

281 To determine whether IL-1Rn modulated immune populations in the airway of the lung during
282 treatment, bronchoalveolar lavages (BAL) were acquired prior to the start of treatment and 3
283 weeks post treatment. Innate and adaptive immune cell populations were identified and
284 frequencies were assessed by flow cytometry (Fig. 7A). Frequencies of CD4 and CD8 T cells
285 (CD3+, CD8+ or CD4+) in BAL remained stable and similar in both groups. Although
286 macrophage (CD11b+CD206+) populations were relatively unchanged, there was a significant
287 reduction in neutrophil (CD11b+, Calprotectin+) frequency in the BAL after 3 weeks of treatment
288 (pooled groups) ($p=0.0098$). This observation was similar to that observed in mice (Fig 2A). To
289 determine whether the cytokine milieu in the airways changed during treatment, a subset of 3
290 animals per group were chosen at random for analysis by multi-plex using 10X concentrated
291 BAL fluid (Fig. 7B). Given the small subset, statistical analysis was performed on combined
292 treatment groups to only compare pre and post treatment changes. We assessed IL-1β and IL-
293 1RA as IL-1Rn may modulate this pathway and saw no significant changes after treatment (IL-
294 1β $p=0.1562$, IL-1RA $p=0.1250$). Interferon-inducible T cell alpha chemoattractant (I-TAC) is
295 upregulated in response in interferons and IL-1 and is generally an indicator of inflammation,
296 which also trended towards reduced levels post treatment, however was not statistically
297 significant ($p=0.0625$). IL-8, a neutrophil chemoattractant, was significantly reduced after
298 treatment, mirroring the reduction in neutrophil frequency observed by flow cytometry and
299 mouse data. These data suggest that treatment with either LZD or LZD+IL-1Rn rapidly reduces
300 inflammatory signatures associated with TB disease in the airways.
301

302 **IL-1 blockade modulates granuloma specific responses and healing dynamics**

303 To determine whether IL-1Rn modulated immune responses at the site of infection, we chose at
304 random 5 granulomas per animal (25 per treatment group) and performed a multi-plex analysis
305 of granuloma supernatants (Fig. 8A). There were no significant differences in IL-1β, IL-1RA, or

306 IL-18 levels, which are associated with the IL-1 pathway. IL-2 and IL-17 are correlated with
307 protective immune responses during TB (26); there was a trend for higher IL-2 levels in LZD+IL-
308 1Rn treatment and a statistically significant increase in IL-17a in LZD+IL-1Rn treated animals.
309 G-CSF/CSF-3 levels were significantly higher in LZD+IL-1Rn treated granulomas, providing
310 further evidence of IL-1Rn immune modulation. The IL-1 pathway is associated with fibrosis,
311 which increases in granulomas during drug treatment. IL-17 and G-CSF are also associated
312 with fibrosis (27). Granulomas suitable for histological analysis were evaluated by a blinded
313 pathologist and lesions were categorized based on treatment groups and descriptive qualities
314 (Fig. 8B). Of lesions acquired from LZD only animals, 71.43% were deemed fibrotic (n= 40/56),
315 while those with the addition of IL-1Rn had 84.78% fibrotic lesions (n=39/46) with no significant
316 difference in frequency of fibrotic lesions between treatment groups. We also compared the
317 number and frequency of granulomas that were deemed necrotizing or non-necrotizing ("other"
318 indicates neither categorization). Granulomas from LZD+IL-1Rn treated animals had
319 significantly more non-necrotizing granulomas (73.91%, n=34/46), compared to those from LZD
320 alone treated macaques (46.43%, n=26/56). The proportion of necrotizing granulomas was
321 significantly lower in the LZD+IL-1Rn treatment group (13.04%, n=6/56) compared to LZD alone
322 (30.36%, n=17/56) (p=0.0151). These data suggest that addition of IL-1Rn may influence
323 antibiotic-associated healing dynamics of granulomas.
324

325 ## Discussion

326 HDTs are a tantalizing solution in combating drug-resistant pathogens, however the
327 complexities of host-pathogen interactions and host variability call for rigorous pre-
328 clinical testing before implementation in humans. Here, we sought to determine the
329 efficacy and safety of an HDT for TB comprised of LZD and IL-1Rn. IL-1 has a complex
330 role during TB, as IL-1 is important for early control of infection, yet damaging in later

331 stages of disease. To validate the safety of IL-1Rn in this context, we first assessed the
332 effects of IL-1Rn on TB disease progression in mice. Using αIL-1R1 blockade,
333 antagonism of IL-1R1 did not exacerbate disease and reduced PMN infiltrates which are
334 associated with pathological inflammation. While inhibition of IL-1 signaling during the
335 early stages of infection has been shown to potentiate disease, the beneficial effect of
336 IL-1 inhibition that we observed in multiple mouse models of TB highlights the generally
337 pathological role for this cytokine during established infections (7, 8).
338 When co-administered with LZD, blockade of IL-1R1 reduced PMN infiltrates in the
339 mouse models, compared to the antibiotic alone. Similarly, IL-1Rn reduced
340 inflammation in the granulomas of macaques, as well as overall lung inflammation as
341 assessed by PET CT, but did not significantly enhance bacterial clearance. A trend of
342 lower CFU in CFU+ lymph nodes (p=0.0965) was observed from macaques treated with
343 LZD+IL-1Rn compared to LZD alone. We hypothesize that IL-1Rn may reduce
344 inflammation in tissues to allow for enhanced penetration of LZD to reduce bacterial
345 burden in tissues. Given that lymph nodes are a site of Mtb persistence, this finding is
346 worth further exploration as a means of potentially enhancing drug penetration in
347 tissues (28).
348
349 In the BAL, we observed a decrease in neutrophils (PMNs) during HDT and a
350 corresponding decrease in IL-8 in both treatment group (LZD or LZD+IL-1Rn), indicating
351 LZD alone was efficacious in reducing PMN inflammatory signatures, likely due to the
352 reduction in bacterial burden. In granulomas, levels of IL-1β, IL-1RA and IL-18 were not
353 affected by IL-1Rn treatment in the subset examined. As IL-1Rn does not affect

354 inflammasome formation and function, only IL-1R1 signal transduction, it is not
355 surprising that IL-1β and IL-18 production were not affected by IL-1Rn. Of the 30
356 cytokines and chemokines assessed, IL-2, IL-17A and G-CSF were the most modulated
357 after IL-1Rn treatment. IL-2 and IL-17A have protective functions during TB and are
358 primarily expressed by T cells (26). While IL-1β has been reported to enhance IL-17A
359 production by T cells in mice, these studies primarily have utilized model-antigen
360 systems while our study reflects a chronic infection model (29). IL-1 is known to be
361 protective early during Mtb infection while exacerbating pathology during later infection,
362 highlighting that the effects of IL-1 on adaptive immunity are complex and likely
363 dependent on the host and infection model. G-CSF was increased in granulomas from
364 LZD+IL-1Rn treated macaques which, combined with our observations of reduced PMN
365 infiltrates in mouse lungs and macaque airways, indicated a paradoxical role of G-CSF
366 as a neutrophil production and differentiation factor (30). However, in a model of LPS-
367 induced lung injury it was shown that G-CSF blockade induced accumulation of PMNs
368 and increased inflammation in the lungs, indicating pulmonary inflammation may not
369 follow dogmatic rules of canonical inflammatory pathways (30).
370
371 Fibrosis is modulated by the IL-1 pathway, however while fibrosis is associated with
372 granuloma healing, lung fibrosis can cause secondary complications after TB disease
373 resolution (2) . We have shown in previous studies that drug therapy for TB induces
374 fibrotic healing in granulomas (31, 32). Therefore, we assessed whether IL-1Rn was
375 associated with changes in granuloma pathology. While we did not observe a
376 significant difference in the frequency of fibrotic versus non-fibrotic granulomas

377 (p=0.1531), there was a significant decrease in necrotizing granulomas when IL-1Rn
378 was added to LZD therapy. Thus, although there is no synergistic effect between IL-
379 1Rn and LZD in promoting fibrosis associated with drug clearance, the reduction in
380 neutrophils could skew granuloma resolution towards a non-necrotizing, fibrotic lesion.
381
382 We also assessed LZD-associated bone marrow suppression and reversal with IL-1Rn
383 therapy. We designed our HDT to match the current FDA guidelines for LZD and IL-
384 1Rn schedules, which resulted in a lack of observable bone marrow suppression in
385 macaques. In mice however, LZD-induced bone marrow suppression was reduced with
386 the addition of IL-1R1 antagonists, supporting our initial hypothesis. The role of IL-1
387 signaling is consistent with the ability of IL-1 to suppress erythropoiesis in mice by
388 reducing the number of progenitors (33). The remaining deficit in erythropoiesis during
389 IL-1 blockade could reflect either incomplete inhibition by IL-1Rn or an independent role
390 of inflammasome activation. Optimizing this effect will require further work to
391 understand the relative roles of IL-1 signaling and inflammasome activation.
392
393 Our data support and extend our previous data in macaques that LZD has excellent
394 efficacy against TB, even as a single-drug given for only 4-weeks, providing additional
395 support for LZD as an antimicrobial for MDR/XDR-TB cases (12). IL-1Rn therapy in
396 conjunction with LZD was successful in reducing TB-associated inflammation with no
397 negative effects on Mtb clearance, however additional studies addressing long-term
398 effects on immune responses and TB disease resolution are needed. Anakinra (IL-1Rn)
399 is already FDA-approved for adult and pediatric use in other inflammatory disorders; our

400 data provide pre-clinical evidence that IL-1Rn could be a potential therapy for cases of
401 severe TB to quell excessive inflammation and improve standard therapies. Our study
402 highlights the potential of HDTs for TB but also the necessity of assessment in
403 translational models prior to implementation in human trials.
404

405 ## Methods

406 **Ethics Statement**

407 All experimental manipulations, protocols, and care of the animals were approved by
408 the University of Pittsburgh School of Medicine Institutional Animal Care and Use
409 Committee (IACUC). The protocol assurance number for our IACUC is A3187-01. Our
410 specific protocol approval numbers for this project are 15117082, 16017370, 18124275,
411 13011368 and 16027525. The IACUC adheres to national guidelines established in the
412 Animal Welfare Act (7 U.S.C. Sections 2131 - 2159) and the Guide for the Care and
413 Use of Laboratory Animals (8th Edition) as mandated by the U.S. Public Health Service
414 Policy.
415 All macaques used in this study were housed at the University of Pittsburgh in rooms
416 with autonomously controlled temperature, humidity, and lighting. Animals were singly
417 housed in caging at least 2 square meters that allowed visual and tactile contact with
418 neighboring conspecifics. The macaques were fed twice daily with biscuits formulated
419 for nonhuman primates, supplemented at least 4 days/week with large pieces of fresh
420 fruits or vegetables. Animals had access to water *ad libitem*. Because our macaques
421 were singly housed due to the infectious nature of these studies, an enhanced
422 enrichment plan was designed and overseen by our nonhuman primate enrichment

423 specialist. This plan has three components. First, species-specific behaviors are
424 encouraged. All animals have access to toys and other manipulata, some of which will
425 be filled with food treats (e.g. frozen fruit, peanut butter, etc.). These are rotated on a
426 regular basis. Puzzle feeders foraging boards, and cardboard tubes containing small
427 food items also are placed in the cage to stimulate foraging behaviors. Adjustable
428 mirrors accessible to the animals stimulate interaction between animals. Second,
429 routine interaction between humans and macaques are encouraged. These interactions
430 occur daily and consist mainly of small food objects offered as enrichment and adhere
431 to established safety protocols. Animal caretakers are encouraged to interact with the
432 animals (by talking or with facial expressions) while performing tasks in the housing
433 area. Routine procedures (e.g. feeding, cage cleaning, etc) are done on a strict
434 schedule to allow the animals to acclimate to a routine daily schedule. Third, all
435 macaques are provided with a variety of visual and auditory stimulation. Housing areas
436 contain either radios or TV/video equipment that play cartoons or other formats
437 designed for children for at least 3 hours each day. The videos and radios are rotated
438 between animal rooms so that the same enrichment is not played repetitively for the
439 same group of animals.
440 All animals are checked at least twice daily to assess appetite, attitude, activity
441 level, hydration status, etc. Following *M. tuberculosis* infection, the animals are
442 monitored closely for evidence of disease (e.g., anorexia, weight loss, tachypnea,
443 dyspnea, coughing). Physical exams, including weights, are performed on a regular
444 basis. Animals are sedated prior to all veterinary procedures (e.g. blood draws, etc.)
445 using ketamine or other approved drugs. Regular PET/CT imaging is conducted on

446 most of our macaques following infection and has proved very useful for monitoring
447 disease progression. Our veterinary technicians monitor animals especially closely for
448 any signs of pain or distress. If any are noted, appropriate supportive care (e.g. dietary
449 supplementation, rehydration) and clinical treatments (analgesics) are given. Any
450 animal considered to have advanced disease or intractable pain or distress from any
451 cause is sedated with ketamine and then humanely euthanatized using sodium
452 pentobarbital.
453
454
455 **Mice, infection and treatment**
456 C57BL/6 (stock no. 000664), *Nos2*$^{-/-}$ (B6.129P2-Nos2^{tm1Lau}/J, stock no. 002609), C3HeB/FeJ
457 (stock no. 00658), and *Nlrp3*$^{-/-}$ (B6.129S6-*Nlrp3*^{tm1Bhk}/J, stock no. 021302) were purchased from
458 the Jackson Laboratory. Breeding pairs of Caspase-1/11 double knock out mice were kindly
459 provided by Prof. Katherine Fitzgerald of the Department of Infectious Diseases at University of
460 Massachusetts (UMASS) Medical School and bred in house. Mice were housed under specific
461 pathogen-free conditions, and in accordance with the UMASS Medical School, IACUC guidelines.
462 All mouse strains used in this study were of C57BL/6 background unless otherwise indicated.
463
464 The wild type strain of *M. tuberculosis* (Mtb) Erdman was used in these studies. Bacteria were
465 cultured in 7H9 medium containing 0.05% Tween 80 and OADC enrichment (Becton Dickinson).
466 For infections, mycobacteria were suspended in phosphate-buffered saline (PBS)-Tween 80
467 (0.05%); clumps were dissociated by sonication, and ~100 CFU were delivered via the respiratory
468 route using an aerosol generation device (Glas-Col, Terre Haute, IN). At indicated time points
469 mice were treated with 200mg/kg of Linezolid (LZD). These drugs were prepared in 0.5%
470 carboxymethyl cellulose (CMC) and Polyethylene glycol 300 solution as the vehicle. Cohorts of

471 mice were treated with anti-IL-1R1 antibody (InVivoMab, anti-mouse IL-1R, Clone JAMA147,
472 BioXcell), or human recombinant IL-1 receptor antagonist (IL-1Rn, Kineret™) either alone or in
473 combination with LZD. 0.5% CMC and Polyethylene glycol was used as vehicle control. All
474 antibiotic treatment was done by daily oral gavage. Anti-IL-1R1 (100ug/mouse/0.2mL) was
475 administered every alternate day by subcutaneous and intraperitoneal route. IL-1Rn (Kineret) was
476 administered (25mg/kg/mouse) everyday by subcutaneous route.
477
478 **Macaque pharmacokinetic study and analytical method.**
479 Uninfected macaques designated for other studies (n=3) were given 20mg/kg or 40mg/kg by oral
480 gavage and plasma acquired at 0, 5, 19, 15, 20, 25 and 30 hours post LZD administration. High
481 pressure liquid chromatography coupled to tandem mass spectrometry (LC/MS-MS) analysis was
482 performed on a Sciex Applied Biosystems Qtrap 4000 triple-quadrupole mass spectrometer
483 coupled to an Agilent 1260 HPLC system to quantify LZD in macaque plasma. LZD
484 chromatography was performed on an Agilent Zorbax SB-C8 column (2.1x30 mm; particle size,
485 3.5 µm) using a reverse phase gradient elution. Milli-Q deionized water with 0.1% formic acid
486 was used for the aqueous mobile phase and 0.1% formic acid in acetonitrile for the organic mobile
487 phase. Multiple-reaction monitoring (MRM) of parent/daughter transitions in electrospray positive-
488 ionization mode was used to quantify the analytes. Sample analysis was accepted if the
489 concentrations of the quality control samples were within 20% of the nominal concentration. Data
490 processing was performed using Analyst software (version 1.6.2; Applied Biosystems Sciex).
491 Neat 1 mg/mL DMSO stocks for all compounds were serial diluted in 50/50 Acetonitrile water to
492 create standard curves and quality control spiking solutions. 20 µL of neat spiking solutions were
493 added to 20 µL of drug free plasma or control tissue homogenate, and extraction was performed
494 by adding 180 µL of Acetonitrile/Methanol 50/50 protein precipitation solvent containing the
495 internal standard (10 ng/mL verapamil & deuterated LZD-d3). Extracts were vortexed for 5

496 minutes and centrifuged at 4000 RPM for 5 minutes. 100 µL or supernatant was transferred for
497 LC-MS/MS analysis and diluted with 100 µL of Milli-Q deionized water.
498 Rhesus macaque plasma (Lithium Heparin, Bioreclamation IVT, NY) was used as a surrogate to
499 cynomolgus macaque plasma to build standard curves. LZD-d3 internal standard and verapamil
500 were purchased from Toronto Research Chemical. The lower and upper limits of quantitation
501 (LLOQ and ULOQ) were 1 ng/mL and 50,000 ng/mL respectively. The following MRM transitions
502 were used for LZD (338.00/235.00), LZD-d3(341.20/297.20), and verapamil (455.40/165.20).
503
504 **Macaques, infection and treatment**
505 All housing, care, and experimental procedures were approved by the University of Pittsburgh
506 School of Medicine Institutional Animal Care and Use Committee (IACUC). Examination of
507 animals was performed in quarantine to assess physical health and confirmation of no previous
508 *M. tuberculosis* infections as previously described (34). Cynomolgus macaques (*Macaca*
509 *fascicularis*) (N=10) were purchased for this study from (Valley Biosystems). Bone marrow
510 control (non-drug treated) samples were taken from Mtb-infected cynomolgus macaques in
511 unrelated ongoing studies (N=5). For the current study, all 10 animals were infected
512 bronchoscopically with 12 CFU of Mtb strain Erdman. After active disease developed (3-5
513 months), NHPs were randomized to LZD only (N=5) or LZD+IL-1Rn (N=5) treatment groups. For
514 randomization, macaques were paired based on total FDG activity in lungs (a surrogate for total
515 thoracic CFU), and then assigned to treatment by coin flip (20). LZD was administered twice a
516 day orally with food (30mg/kg), while IL1-Rn was given at 2mg/kg once each day by
517 subcutaneous injection. All animal data are provided in Supplementary Table 1. Medication
518 compliancy was monitored at every administration and pharmacokinetic analysis performed at
519 select times. Drug treatments were administered for 4 weeks prior to necropsy.
520 Bronchoalveolar lavages (BAL) were performed prior to drug-treatment and 3 weeks-post start
521 of treatment for CFU, flow cytometry and multiplex assays.

522

523 **Macaque PET/CT Imaging**

524 Positron emission tomography (PET) with computed tomography (CT) imaging was performed
525 with 2-deoxy-2-[^{18}F]-D-deoxyglucose (FDG) throughout the study as previously described (19).
526 Serial scans were performed throughout the study to track disease progression and changes
527 during drug treatment. Total FDG activity of the lungs was measured over the course of
528 infection and drug treatment as previously described (19). Granulomas identified on scans were
529 denoted, measured (mm) and standard uptake values (SUVR) were determined to assess
530 metabolic activity, a readout for inflammation. SUVR values were normalized to muscle and
531 SUVR and size measurements were determined at each scan over time to compare pre-and
532 post-drug treatment. Each animal was scanned prior to necropsy to identify granulomas for
533 matching at necropsy; granulomas $\geq$ 1mm are distinguishable by PET/CT.

534

535 **Macaque Necropsy**

536 Necropsies were performed as previously described. In short, multiple tissues (granulomas, lung
537 lobes, thoracic lymph nodes, peripheral lymph nodes, liver, spleen, bone marrow) were excised
538 and homogenized into single-cell suspensions for assessment of bacterial burden and
539 immunological assays. Granulomas were individually excised (PET/CT identified and others not
540 identified on scans) and split (size permitting) with one-half for homogenization and single cell
541 suspension and the other half processed for histological analysis. Bone marrow samples were
542 obtained from the sternum, with a portion sent for histological analysis while single cell
543 suspensions were acquired as previously described (35). Bacterial burden was assessed from
544 each tissue by plating serial dilutions on 7H11 agar plates and incubated at 37°C in 5% CO_2 for
545 21 days before enumeration of Mtb CFU.

546

547 **Flow cytometry and Immunoassays**

548 **Mice**. Single cell suspensions were prepared from the infected mouse organs. Briefly, lung tissue
549 was digested with Collagenase type IV/DNaseI and passed through 40 μm cell strainers to obtain
550 single cell suspension. Red blood cells were lysed using Tris-buffered Ammonium Chloride (ACT)
551 Non-specific antibody binding sites were blocked by Fc-Block CD16/32 (Clone 93, cat. no.
552 101319) and the cells were stained with anti-CD3-PE (Clone 17A2, cat. no. 100205), anti-CD11b-
553 PerCP Cy5.5 (Clone M1/70, cat. no.101227), anti-Ly-6G-FITC (Clone 1A8, cat. no.127605), anti-
554 Ly-6C-PE (Clone HK1.4, cat. no.128007), anti-Gr1-APC (Clone RB6-8C5, cat. no.108411), anti-
555 Ter119-PE (Clone TER119, cat. no.116208), anti-CD71-FITC (clone RI7217, cat. no. 113806).
556 Antibodies were purchased from BioLegend. All analyses were performed on live cells only after
557 staining them with fixable live dead stain conjugated with eFlour780, purchased from
558 eBiosciences. All the staining was done according to the manufacturer's instructions. Lung,
559 spleen and bone marrow cells were surface stained for 30 minutes at room temperature, fixed for
560 20 minutes at 4^0C using the Cytofix buffer (BD-Biosciences, cat. no. 554655). Data were acquired
561 in a BD LSRII flow cytometer in the flow cytometry core facility at UMASS medical school and
562 analyzed with FlowJo Software (Treestar, Inc.). Gating strategies are provided in applicable
563 figures.
564 **Macaques.** Single cell suspensions acquired from homogenization of granulomas, lung lobes
565 and lymph nodes were subjected to intracellular cytokine staining (ICS). Prior to staining, cells
566 were incubated in RPMI 1640 containing 1% HEPES, 1% L-glutamine, 10% human AB serum,
567 and 0.1% brefeldin A (Golgiplug; BD Biosciences) for 3 h at 37°C in 5% CO_2. After viability
568 staining (Invitrogen), surface antigens and intracellular cytokines were assessed using standard
569 protocols. Surface markers include CD3 (SP34-2; BD Pharmingen), CD4 (L200; BD Horizon),
570 CD8 (RPA-T8; BD Horizon) for T cells and CD11b (ICRF44; BD Pharmingen), CD206 (19.2; BE
571 Pharmingen) for macrophages/neutrophils. Calprotectin (27E10; ThermoFisher) was stained
572 intracellularly to identify neutrophils. For bone marrow, single cell suspensions underwent red
573 blood cell lysis (BD Pharm Lyse) before incubation in alpha-MEM + 10% Stasis™ FBS (Gemini

574 Bio-Products) + MitoTracker™ Red CMXRos (Invitrogen) for 30 minutes to stain for membrane
575 potential of mitochondria. Cells were then stained for viability (Invitrogen) and surface stained
576 to distinguish erythroid progenitor populations by CD34 (581; Biolegend), CD235a (HIR2; BD
577 Pharmingen), CD71 (L01.1; BD Pharmingen) and CD45 (D058-1283; BD Pharmingen). All
578 samples were acquired on an LSR II (BD) and analyzed with FlowJo Software (Treestar, Inc.).
579 Gating strategies are provided in applicable figures.
580 For the multiplex assays, all samples and supernatants were stored at -80°C from time of
581 necropsy until time of assay. Five representative granuloma supernatants were randomly
582 selected from each animal using JMP Pro v12 (SAS Institute Inc.). Supernatants were thawed
583 and filtered with a 0.22uM syringe filter to remove infectious bacteria and debris, then kept on
584 ice throughout the assay. For BAL samples, supernatants were concentrated using regenerated
585 cellulose centrifugal filter tubes (3,000 NMWL, Millipore Sigma) to a final 10X concentration
586 (5mL to 0.5mL). Both granuloma and BAL supernatants were evaluated with a ProcartaPlex
587 multiplex immunoassay (Invitrogen) that assesses thirty cytokines and chemokines specific for
588 NHPs. We followed the manufacturer's protocol with one modification in which we diluted the
589 standard out an extra dilution to increase the range of detection. Results were analyzed by a
590 BioPlex reader (BioRad).
591
592 **Histopathology and immunofluorescence**
593 **Mice.** Lung tissues were fixed in 10% buffered formalin and embedded in paraffin. Five
594 micrometer-thick sections were stained with hematoxylin and eosin (H&E). Tissue staining was
595 done by the Diabetes and Endocrinology Research Center histopathology core facility at the
596 University of Massachusetts Medical School or immunology core facility of Albany medical
597 college, NY. Brightfield images were acquired in Abaxis VETSCAN HD microscope.
598 Paraffin embedded lung tissue sections were cut at 5 µm thickness, mounted on ultraclean glass
599 slides covered in silane, deparaffinized, then dehydrated and rehydrated using the following

600 steps: Ethanol solutions (30, 50, 70, 90, 95 and 100 % for 3 min each), xylenes (2 different
601 solutions for 10 min each) and ethanol solutions (100, 95, 90, 70, 50 and 30 for 3 min each). The
602 slides were washed once in Tris buffer saline (TBS) for 5 min. Slices were subjected to antigen
603 retrieval by boiling in sodium citrate buffer at pH=6.0 for 20 min and incubated in 0.1% Triton-X
604 100 for 5 min. Slices were removed and allowed to equilibrate to room temperature for at least
605 20 min, and rinsed with distilled water. Tissue sections were blocked (blocking solution; 0.5 M
606 EDTA, 1% BSA, in PBS) and incubated overnight in primary antibodies against the proteins
607 related to our studies. Sections were stained for nuclei (DAPI, blue staining), anti-mouse CD3e
608 (cat.no. ab16669, green staining), anti-mouse Ly-6G (clone 1A8, cat. no. 127602) to identify
609 neutrophil granulocytes (Cy3, red staining). As controls, pre-immune serum and isotype matched
610 controls were used. After incubation, the tissues were washed several times with sterile TBS at
611 room temperature and incubated in the respective secondary antibodies (anti-rabbit conjugated
612 to Alexa-488, anti-rat conjugated to Cy3) for at least 2h at room temperature. Tissue sections
613 were mounted using Prolong Gold Antifade reagent (Invitrogen, grand Island, NY) with DAPI, and
614 the tissue sections were examined in ECHO Revolve 4 microscope. Isotype matched control
615 antibodies were used for checking antibody specificity.
616 **Macaques**. As previously described, samples acquired at necropsy were formalin fixed,
617 paraffin embedded, cut into ~5μm serial sections and stained with H&E (34). A study-blinded
618 veterinary pathologist assessed and characterized each granuloma, indicating size, type,
619 distribution and cellular composition. Sterna for bone marrow analysis were excised and
620 formalin fixed then transected longitudinally into 1 to 2 sternebral unites and placed in Cal-Ex
621 Hydrochloric acid decalcification solution for 2-4 hours. Upon removal, specimens were washed
622 and trimmed to test for adequate mineral removal, then submitted for routine tissue processing
623 with other tissue specimens as described above.
624
625 **Statistical Analysis**

626 **Mouse studies:** Equal variance between samples was assessed by Brown-Forsythe test.
627 Experiments in which variances were equivalent were analyzed by one-way ANOVA with
628 Sidak's multiple comparisons test. Those with unequal variances were analyzed by Welch
629 ANOVA and Dunnett's multiple comparisons test. P values < 0.05 was considered significant.
630 **Macaque studies:** Nonparametric U tests (Mann-Whitney) were performed for two-group
631 comparisons and Kruskal-Wallis tests were performed for three-group comparisons as indicated
632 on data sets with non-normal distributions. Wilcoxon signed rank tests were performed for
633 matched pairs. Fisher's exact test was run on any categorical data. P values < 0.05 were
634 considered significant. Total lung FDG activity was $\log_{10}$-transformed. A two-way ANOVA was utilized
635 to test whether treatment or time (or an interaction between these factors) had an effect on total
636 lung inflammation. Dunnett's multiple comparison tests were then used to compare each time
637 point to pre-drug treatment within each treatment group. Statistical analyses were performed in
638 GraphPad Prism 8 (GraphPad Software, San Diego, CA). A regression equation created from
639 control animals from previous studies was used to create a 95% prediction interval for total
640 thoracic bacterial burden using total lung FDG activity on the scan just before drug treatment
641 (20). The lower and upper bounds and the mean of this prediction interval were subtracted from
642 each animal's total CFU to estimate change in CFU over the course drug treatment. All
643 statistical analyses are referenced in the corresponding figure legends.
644

645 ## Acknowledgements

646 These studies were funded by NIH UH2AI122295 (JLF and CMS). CGW was supported by NIH
647 T32AI049820. We thank all members of the Flynn, Sassetti, Mattila, and Lin laboratories for
648 their collaborative efforts during this study. We are grateful for intellectual contributions from Dr.
649 Clifton Barry III and Dr. Robert Wilkinson. Special thanks to all the veterinary and research staff
650 for their efforts, expertise and dedication to these studies.

651

652 ## References

653 1. WHO. Global Tuberculosis Report 2018. 2018.

654 2. Pasipanodya JG, Miller TL, Vecino M, Munguia G, Garmon R, Bae S, et al. Pulmonary
655 impairment after tuberculosis. Chest. 2007;131(6):1817-24.

656 3. Tobin DM. Host-Directed Therapies for Tuberculosis. Cold Spring Harb Perspect Med.
657 2015;5(10).

658 4. Baindara P. Host-directed therapies to combat tuberculosis and associated non-
659 communicable diseases. Microb Pathog. 2019;130:156-68.

660 5. Fremond CM, Togbe D, Doz E, Rose S, Vasseur V, Maillet I, et al. IL-1 Receptor-
661 Mediated Signal Is an Essential Component of MyD88-Dependent Innate Response to
662 Mycobacterium tuberculosis Infection. The Journal of Immunology. 2007;179(2):1178-89.

663 6. Di Paolo NC, Shafiani S, Day T, Papayannopoulou T, Russell DW, Iwakura Y, et al.
664 Interdependence between Interleukin-1 and Tumor Necrosis Factor Regulates TNF-Dependent
665 Control of Mycobacterium tuberculosis Infection. Immunity. 2015;43(6):1125-36.

666 7. Juffermans NP, Florquin S, Camoglio L, Verbon A, Kolk AH, Speelman P, et al.
667 Interleukin-1 signaling is essential for host defense during murine pulmonary tuberculosis. J
668 Infect Dis. 2000;182(3):902-8.

669 8. Mayer-Barber KD, Andrade BB, Barber DL, Hieny S, Feng CG, Caspar P, et al. Innate
670 and adaptive interferons suppress IL-1alpha and IL-1beta production by distinct pulmonary
671 myeloid subsets during Mycobacterium tuberculosis infection. Immunity. 2011;35(6):1023-34.

672 9. Mishra BB, Lovewell RR, Olive AJ, Zhang G, Wang W, Eugenin E, et al. Nitric oxide
673 prevents a pathogen-permissive granulocytic inflammation during tuberculosis. Nat Microbiol.
674 2017;2:17072.

675 10. Mishra BB, Rathinam VA, Martens GW, Martinot AJ, Kornfeld H, Fitzgerald KA, et al.
676 Nitric oxide controls the immunopathology of tuberculosis by inhibiting NLRP3 inflammasome-
677 dependent processing of IL-1beta. Nat Immunol. 2013;14(1):52-60.
678 11. Zhang G, Zhou B, Li S, Yue J, Yang H, Wen Y, et al. Allele-specific induction of IL-1beta
679 expression by C/EBPbeta and PU.1 contributes to increased tuberculosis susceptibility. PLoS
680 Pathog. 2014;10(10):e1004426.
681 12. Maxmen A. Treatment for extreme drug-resistant tuberculosis wins US government
682 approval. Nature 2019.
683 13. Tan TQ, Yogev R. Clinical pharmacology of linezolid: an oxazolidinone antimicrobial
684 agent. Expert Rev Clin Pharmacol. 2008;1(4):479-89.
685 14. Coleman MT, Chen RY, Lee M, Lin PL, Dodd LE, Maiello P, et al. PET/CT imaging
686 reveals a therapeutic response to oxazolidinones in macaques and humans with tuberculosis.
687 Sci Transl Med. 2014;6(265):265ra167.
688 15. Lee M, Lee J, Carroll MW, Choi H, Min S, Song T, et al. Linezolid for treatment of
689 chronic extensively drug-resistant tuberculosis. N Engl J Med. 2012;367(16):1508-18.
690 16. Iyer SS, He Q, Janczy JR, Elliott EI, Zhong Z, Olivier AK, et al. Mitochondrial cardiolipin
691 is required for Nlrp3 inflammasome activation. Immunity. 2013;39(2):311-23.
692 17. Weber A, Wasiliew P, Kracht M. Interleukin-1 (IL-1) pathway. Sci Signal.
693 2010;3(105):cm1.
694 18. Furst DE. Anakinra: review of recombinant human interleukin-I receptor antagonist in the
695 treatment of rheumatoid arthritis. Clin Ther. 2004;26(12):1960-75.
696 19. White AG, Maiello P, Coleman MT, Tomko JA, Frye LJ, Scanga CA, et al. Analysis of
697 18FDG PET/CT Imaging as a Tool for Studying Mycobacterium tuberculosis Infection and
698 Treatment in Non-human Primates. J Vis Exp. 2017(127).

699 20. Maiello P, DiFazio RM, Cadena AM, Rodgers MA, Lin PL, Scanga CA, et al. Rhesus
700 Macaques Are More Susceptible to Progressive Tuberculosis than Cynomolgus Macaques: a
701 Quantitative Comparison. Infect Immun. 2018;86(2).
702 21. Lin PL, Maiello P, Gideon HP, Coleman MT, Cadena AM, Rodgers MA, et al. PET CT
703 Identifies Reactivation Risk in Cynomolgus Macaques with Latent M. tuberculosis. PLoS
704 Pathog. 2016;12(7):e1005739.
705 22. Cadena AM, Fortune SM, Flynn JL. Heterogeneity in tuberculosis. Nat Rev Immunol.
706 2017;17(11):691-702.
707 23. Driver ER, Ryan GJ, Hoff DR, Irwin SM, Basaraba RJ, Kramnik I, et al. Evaluation of a
708 mouse model of necrotic granuloma formation using C3HeB/FeJ mice for testing of drugs
709 against Mycobacterium tuberculosis. Antimicrob Agents Chemother. 2012;56(6):3181-95.
710 24. Lin PL, Coleman T, Carney JP, Lopresti BJ, Tomko J, Fillmore D, et al. Radiologic
711 Responses in Cynomolgus Macaques for Assessing Tuberculosis Chemotherapy Regimens.
712 Antimicrob Agents Chemother. 2013;57(9):4237-44.
713 25. Fung HB, Kirschenbaum HL, Ojofeitimi BO. Linezolid: an oxazolidinone antimicrobial
714 agent. Clin Ther. 2001;23(3):356-91.
715 26. Gideon HP, Phuah J, Myers AJ, Bryson BD, Rodgers MA, Coleman MT, et al. Variability
716 in tuberculosis granuloma T cell responses exists, but a balance of pro- and anti-inflammatory
717 cytokines is associated with sterilization. PLoS Pathog. 2015;11(1):e1004603.
718 27. Borthwick LA. The IL-1 cytokine family and its role in inflammation and fibrosis in the
719 lung. Semin Immunopathol. 2016;38(4):517-34.
720 28. Ganchua SKC, Cadena AM, Maiello P, Gideon HP, Myers AJ, Junecko BF, et al. Lymph
721 nodes are sites of prolonged bacterial persistence during Mycobacterium tuberculosis infection
722 in macaques. PLoS Pathog. 2018;14(11):e1007337.

723 29. Ben-Sasson SZ, Hu-Li J, Quiel J, Cauchetaux S, Ratner M, Shapira I, et al. IL-1 acts
724 directly on CD4 T cells to enhance their antigen-driven expansion and differentiation. Proc Natl
725 Acad Sci U S A. 2009;106(17):7119-24.
726 30. Bajrami B, Zhu H, Kwak HJ, Mondal S, Hou Q, Geng G, et al. G-CSF maintains
727 controlled neutrophil mobilization during acute inflammation by negatively regulating CXCR2
728 signaling. J Exp Med. 2016;213(10):1999-2018.
729 31. DiFazio RM, Mattila JT, Klein EC, Cirrincione LR, Howard M, Wong EA, et al. Active
730 transforming growth factor-beta is associated with phenotypic changes in granulomas after drug
731 treatment in pulmonary tuberculosis. Fibrogenesis Tissue Repair. 2016;9:6.
732 32. Warsinske HC, DiFazio RM, Linderman JJ, Flynn JL, Kirschner DE. Identifying
733 mechanisms driving formation of granuloma-associated fibrosis during Mycobacterium
734 tuberculosis infection. J Theor Biol. 2017;429:1-17.
735 33. Johnson CS, Pourbohloul SC, Furmanski P. Negative regulators of in vivo
736 erythropoiesis: interaction of IL-1 alpha and TNF-alpha and the lack of a strict requirement for T
737 or NK cells for their activity. Exp Hematol. 1991;19(2):101-5.
738 34. Lin PL, Pawar S, Myers A, Pegu A, Fuhrman C, Reinhart TA, et al. Early events in
739 Mycobacterium tuberculosis infection in cynomolgus macaques. Infect Immun. 2006;74(7):3790-
740 803.
741 35. Phuah JY, Mattila JT, Lin PL, Flynn JL. Activated B cells in the granulomas of nonhuman
742 primates infected with Mycobacterium tuberculosis. Am J Pathol. 2012;181(2):508-14.
743

744 **Figures and Figure Legends**

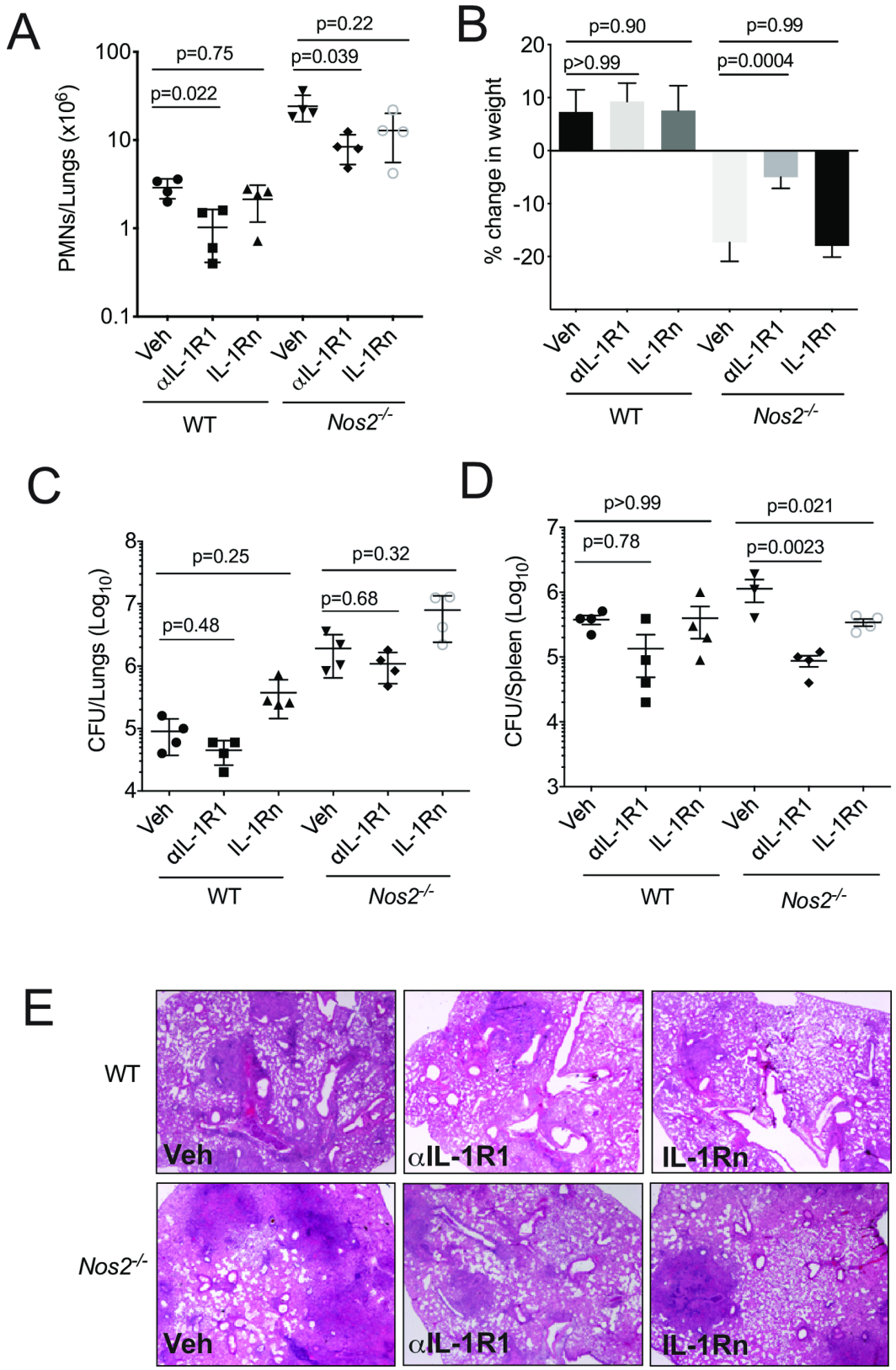
A
PMNs/Lungs (x10^6)
100
10
1
0.1
p=0.75
p=0.022
p=0.22
p=0.039
Veh
αIL-1R1
IL-1Rn
Veh
αIL-1R1
IL-1Rn
WT
Nos2-/-
B
% change in weight
20
10
0
-10
-20
p=0.90
p>0.99
p=0.99
p=0.0004
Veh
αIL-1R1
IL-1Rn
Veh
αIL-1R1
IL-1Rn
WT
Nos2-/-
C
CFU/Lungs (Log10)
8
7
6
5
4
p=0.25
p=0.48
p=0.32
p=0.68
Veh
αIL-1R1
IL-1Rn
Veh
αIL-1R1
IL-1Rn
WT
Nos2-/-
D
CFU/Spleen (Log10)
7
6
5
4
3
p>0.99
p=0.78
p=0.021
p=0.0023
Veh
αIL-1R1
IL-1Rn
Veh
αIL-1R1
IL-1Rn
WT
Nos2-/-
E
WT
Nos2-/-
Veh
αIL-1R1
IL-1Rn
Veh
αIL-1R1
IL-1Rn

745

746 **Figure 1. IL-1 inhibition in susceptible mice reduces inflammation with no effect on lung**

747 **bacterial burden.**

748 Wild type C57BL/6 and *Nos2*$^{-/-}$ mice were infected with Mtb Erdman for 2 weeks, and treated

749 with anti-IL-1R1 (αIL-1R1) or IL-1R1-antagonist (IL-1Rn) for the subsequent 2 weeks. (A) Lung

750 neutrophil (PMN) infiltration was quantified by flow cytometry; (B) Weight loss and (C) CFU in

751 lung and (D) spleen are shown. Data shown (mean ± SD) are representative of two independent

752 experiments. One-way ANOVA with Sidak's multiple comparisons-test was used. N=4 mice per

753 treatment cohorts. (E) Histopathology analysis of a single lung lobe from WT or *Nos2-/-* mice

754 was performed by Hematoxylin-eosin (H&E) staining.

755

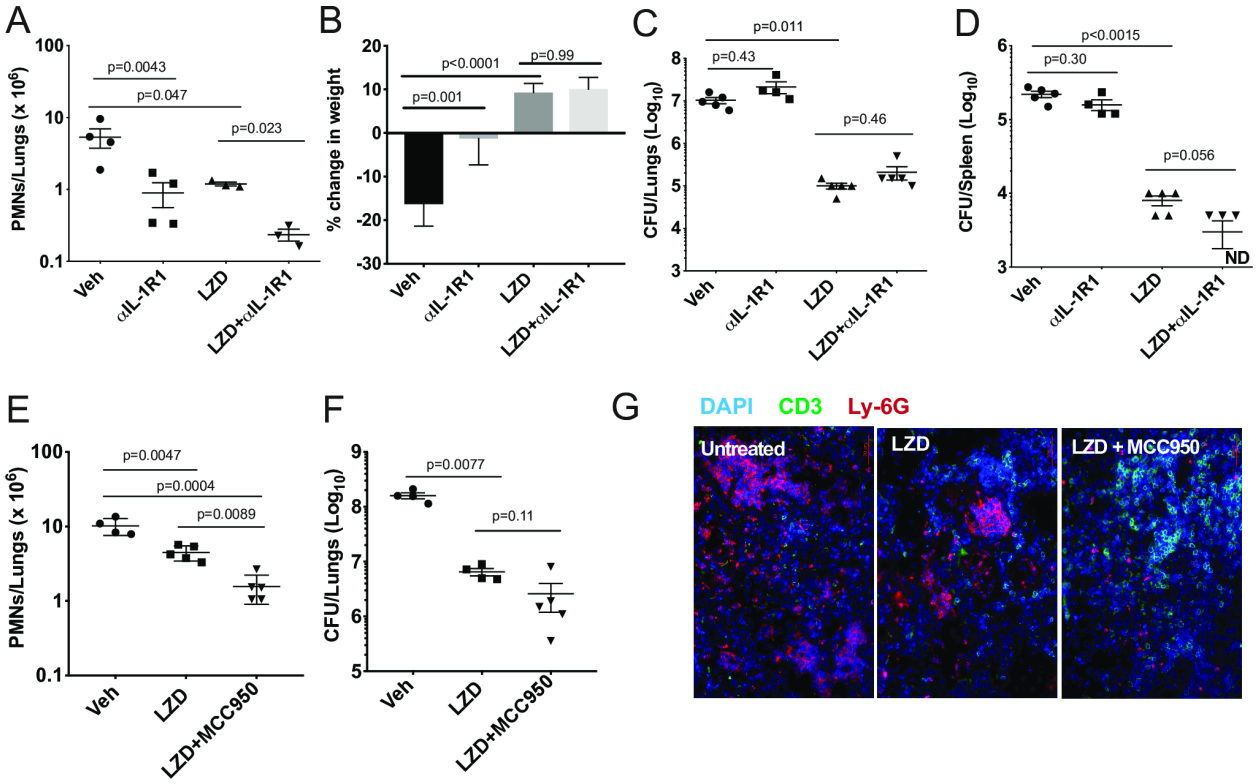

756

757 **Figure 2. IL-1R1 blockade combined with Linezolid ameliorates TB disease.**

758 (A-D) C3HeB/FeJ mice were infected with Mtb Erdman for 4 weeks and treated with linezolid

759 (LZD) and/or anti-IL-1R1 (αIL-1R1) for the following 18 days. (A) Lung neutrophils were

760 quantified by flow cytometry; (B) Percent change in body weight is shown and (C) Bacterial

761 burden in the lung and (D) spleen were quantified as CFU. Data shown (Mean ± SD) are
762 representative of two independent experiments. Welch ANOVA with Dunnett's post-test was
763 used to calculate statistical significance where each treatment group was compared to the
764 vehicle as control group. N=3-5 mice per treatment group. (E-G) C3HeB/FeJ mice were infected
765 with *M. tb* Erdman for 8 weeks and treated with linezolid (LZD) and/or an inhibitor of the NLRP3
766 inflammasome (MCC950) for the following 21 days. (E) Lung neutrophils were quantified by flow
767 cytometry. (F) Bacterial burden in the lung was quantified by CFU. Data shown (Mean ± SD) are
768 from one experiment. One-way ANOVA with Tukey's multiple comparison test was used to
769 calculate the p-value. N=4-5 mice/group. (G) Representative immunofluorescence images of
770 the lungs from different treatment groups. Cell nuclei stained with DAPI (blue), T-cells stained
771 with anti-mouse CD3ε (green) and neutrophils stained with anti-mouse Ly-6G (red).

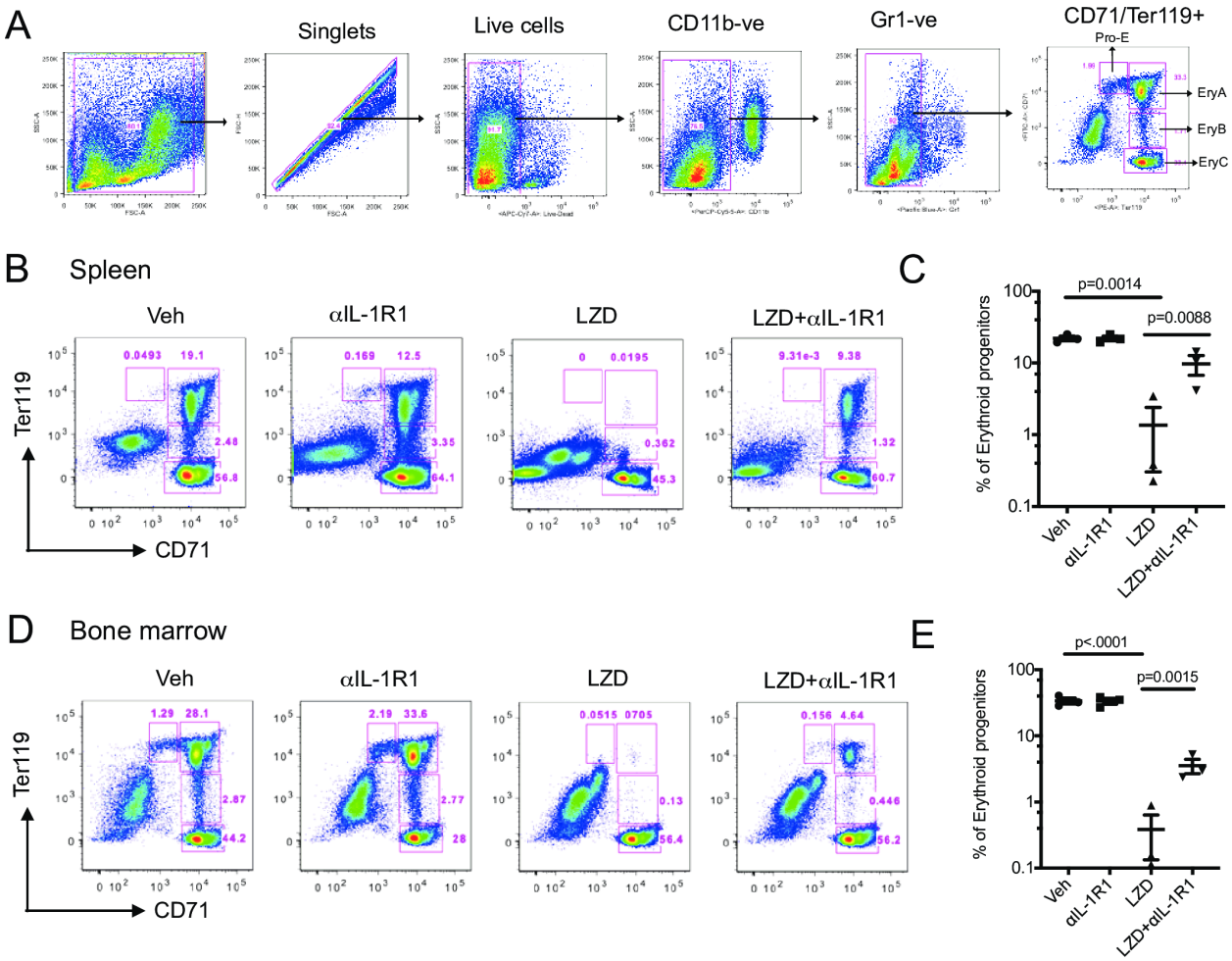

772

773 **Figure 3. Erythropoiesis associated with LZD treatment was partially relieved after IL-**
774 **1R1 blockade.**
775 C3HeB/FeJ mice were infected with Mtb Erdman for 4 weeks, and treated with LZD either alone
776 or in combination with anti-IL-1R1 antibody for the subsequent 18 days. (A) Gating strategy for
777 detecting erythroid progenitors is shown. Erythroid progenitors in the spleen (B-C) and bone
778 marrow (D-E) were quantified by flow cytometry as described in Materials and Methods.
779 Representative flow cytometry plots and percent changes in the early erythroid progenitors (Pro-
780 Ery, EryA, EryB) among different treatment groups are shown. Data shown (Mean ± SD) are
781 from two independent experiments. One-way ANOVA with Dunnett's post-test was applied to
782 calculate the p-value by comparing the mean of each group with that of LZD treated group.
783 N=3-5 mice per group.

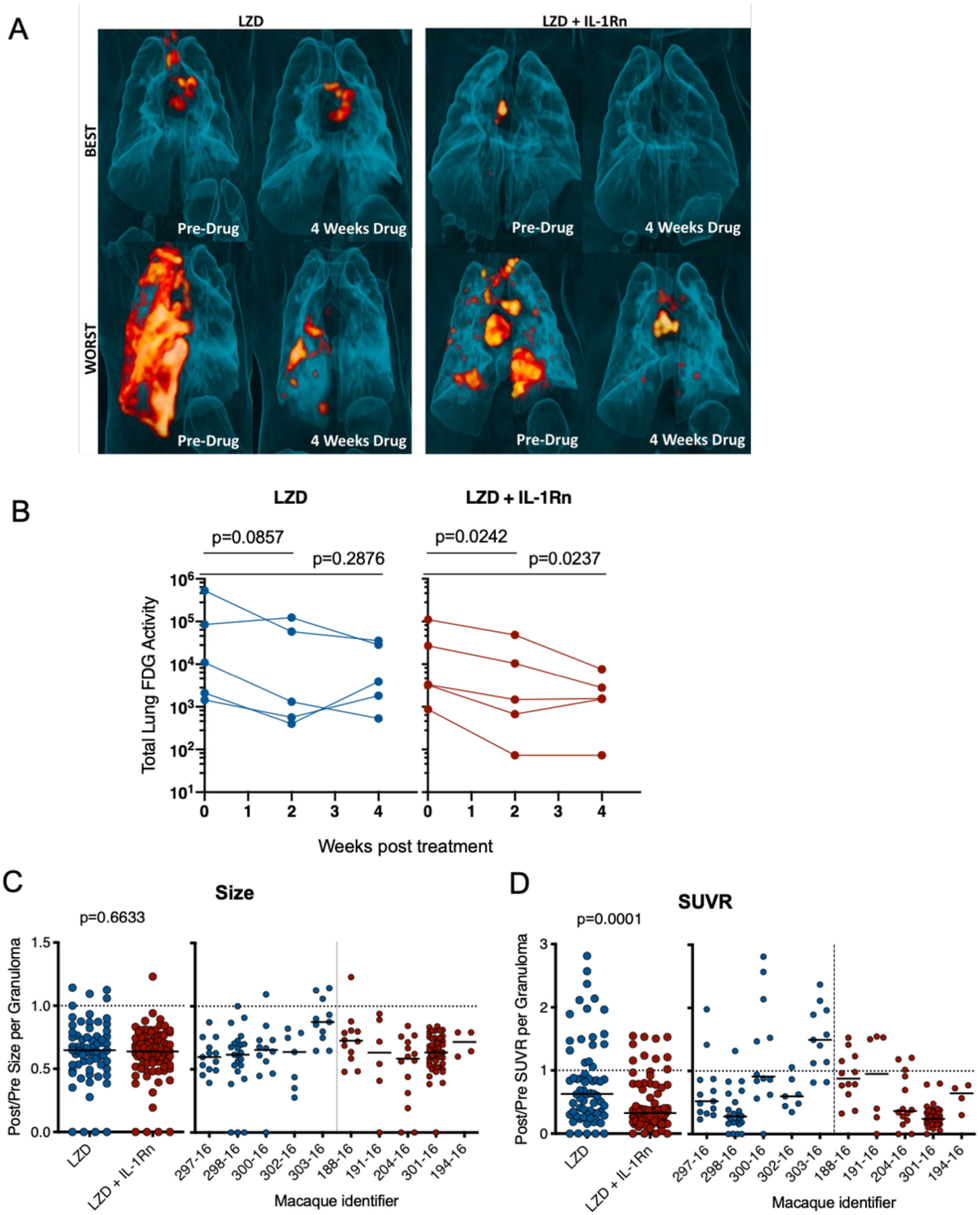

Figure 4. HDT reduces granuloma inflammation by PET/CT in macaques

786 Cynomolgus macaques were infected with *M. tb* Erdman for approximately 4 months (see
787 Supplementary Table 1) and randomized to treatment with LZD or LZD+IL-1Rn for an additional
788 4 weeks. PET/CT scans were performed pre-treatment, 2 and 4 weeks post-treatment with 4
789 week scans as the last prior to necropsy. (A) 3-D renderings of PET/CT scans from pre-
790 treatment and 4 weeks post-treatment are depicted, with "best" and "worst" of each group
791 referring to TB disease prior to drug administration. (B) Total lung FDG activity of each
792 macaque throughout treatment with LZD (left) or LZD+IL-1Rn (right). Two-way ANOVA with
793 Dunnett's adjusted p-values are reported. (C) Individual granulomas were identified pre-
794 treatment and tracked post-treatment by PET/CT. Change in size (by CT) was determined for
795 granulomas from each animal; the left graph is compiled granulomas from each animal in the
796 indicated treatment groups while the right depicts individual animals. (D) Standard uptake value
797 (SUVR) of ^{18}F-FDG was calculated for each granuloma, representing inflammation. Change in
798 SUVR of all granulomas in each groupis depicted on the left, while change in SUVR of
799 granulomas from each individual animal are on the right. For (C) and (D), each data point is
800 representative of one granuloma and the bar represents the median. Mann-Whitney tests
801 determined p values for (C) and (D), with $p<0.05$ considered significant.

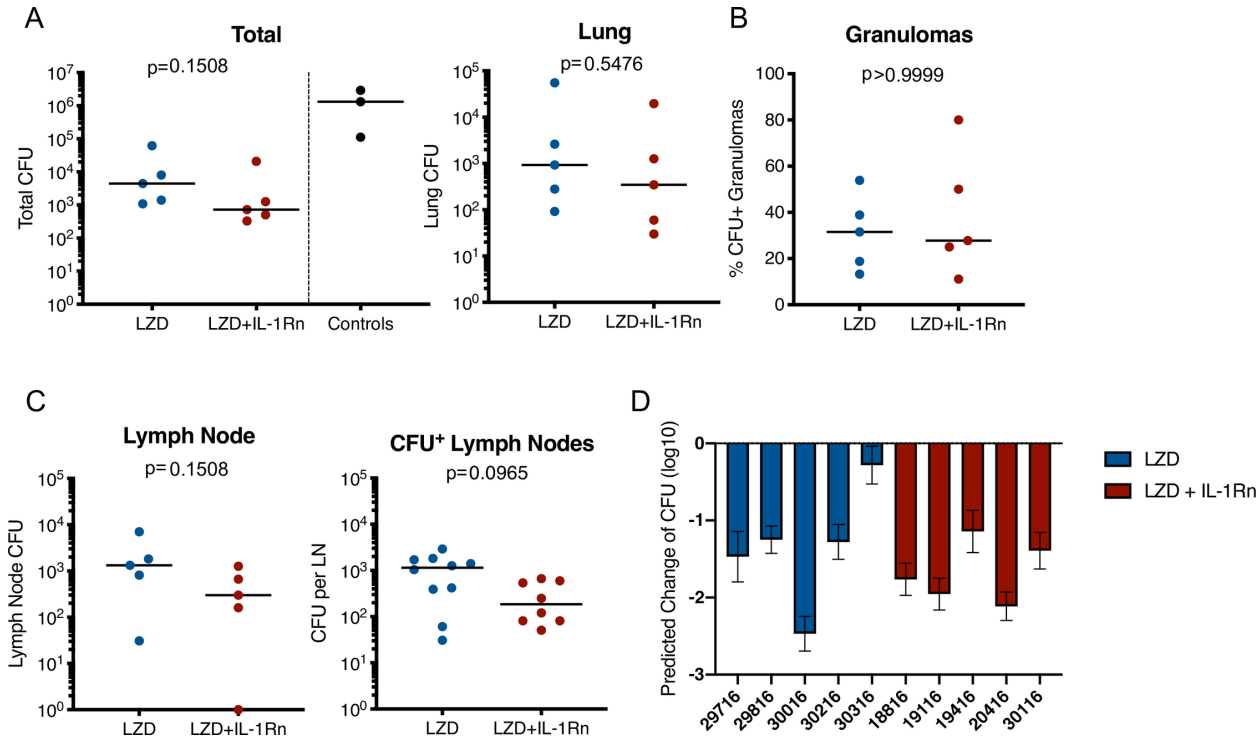

Figure 5. Addition of IL-1Rn does not enhance efficacy of LZD for bacterial killing

Bacterial burden is shown after 4 weeks of LZD (blue) or LZD+IL-1Rn (red) treatment. (A) Total thoracic (lung + lymph nodes) and lung CFU; each data point represents one macaque. Total thoracic CFU from 3 similarly infected untreated historical control macaques (black) are included as reference for untreated CFU at this time point, but excluded from statistical analysis. (B) The percent of all lung granulomas that were CFU+ per monkey. (C) CFU of all thoracic lymph nodes with data points representing CFU from one macaque. CFU+ lymph nodes show the CFU from each thoracic lymph node in any animal that was Mtb+. For (A) and (B), p values were determined by Mann-Whitney test. (C) PET/CT scans from pre-treatment were used to model predicted CFU prior to HDT initiation and compared to actual CFU determined at time of necropsy. The predicted change in CFU was determined by: Actual total thoracic CFU post-treatment– Predicted total thoracic CFU interval (predicted from pre-drug-treatment scan). Bars represent mean of prediction intervals and error whiskers represent the lower and upper bounds of the difference between final total CFU and predicted CFU prior to drug treatment.

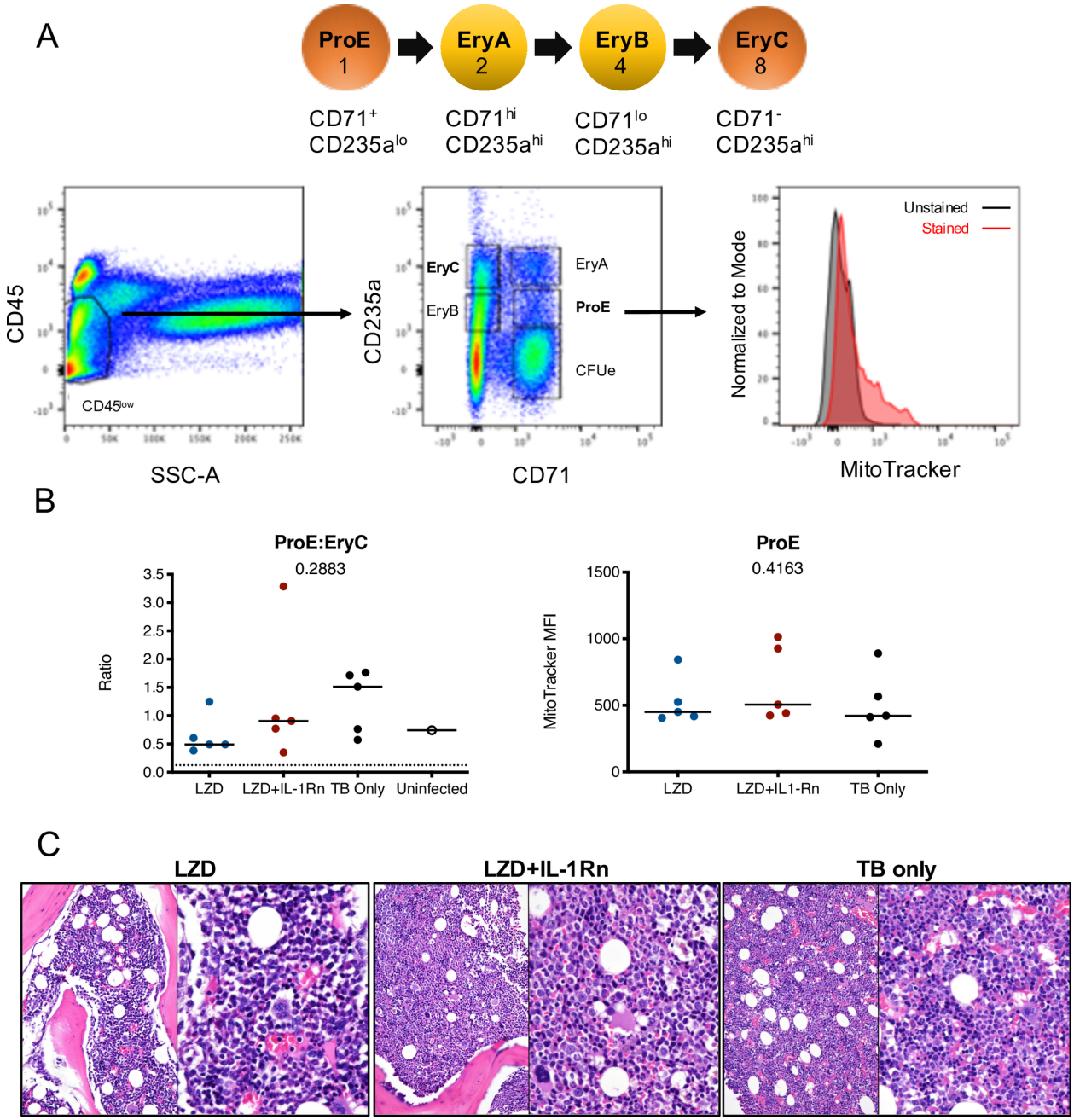

Figure 6. Linezolid-associated bone marrow suppression was not observed in macaques

Bone marrow was acquired from the sternum of all macaques at necropsy after 4 weeks LZD or LZD+IL-1Rn. A portion was used for flow cytometric analysis of erythroid progenitor populations and the rest for histopathology analysis. (A) A schematic of erythropoiesis indicating the stage of differentiation and corresponding expression levels of phenotyping markers (CD235 and CD71) and progenitor ratios (1:2:4:8). Included is the gating strategy to identify progenitor

824 populations and an example of MitoTracker staining. (B) The ProE:EryC ratio (left) of each
825 animal, including untreated TB only macaques (black) from other ongoing unpublished studies.
826 A single uninfected animal (open circle) is shown as reference, the dotted line indicates the
827 homeostatic ratio of 1:8. MitoTracker MFI (right) is shown for each macaque per treatment
828 group. Kruskal-Wallis test was performed to compare the three groups (excluding uninfected
829 macaque) and p values are shown in the graphs. (C) Representative H&E images from sternal
830 bone marrow acquired at necropsy, 20x (left) and 40x (right) are shown.

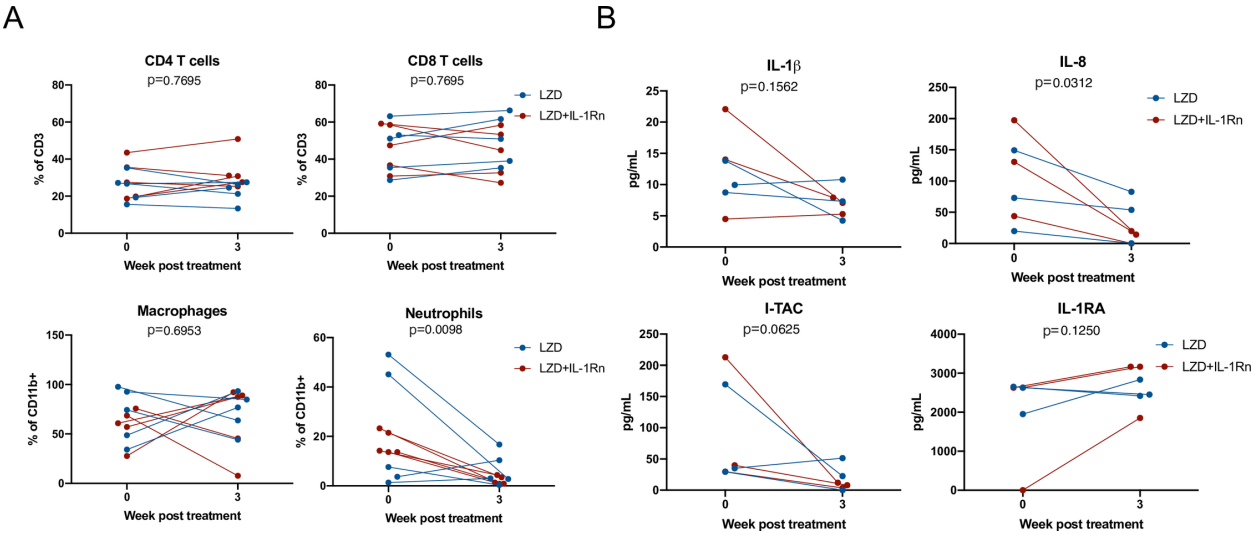

831

832 **Figure 7. HDT reduces inflammatory signatures in BAL**

833 Bronchoalveolar lavages (BAL) were acquired pre-treatment and 3 weeks post-treatment with
834 LZD (blue) or LZD+IL-1Rn (red). (A) Cells were analyzed by flow cytometry to determine
835 frequency changes in CD4 T cells (CD3+CD4+), CD8 T cells (CD3+CD8+), macrophages
836 (CD11b+CD206+) and neutrophils (CD11b+Calprotectin+). Wilcoxon signed rank test was
837 performed to determine differences before and after drug treatment, regardless of group (LZD
838 and LZD+IL-1Rn combined). (B) BAL fluid was concentrated 10X and assessed by multiplex
839 assay for changes in inflammatory cytokines and chemokines for a random subset of samples
840 (n=3 per treatment group). Wilcoxon signed rank test was performed to determine differences
841 before and after drug treatment, regardless of group (LZD and LZD+IL-1Rn combined).

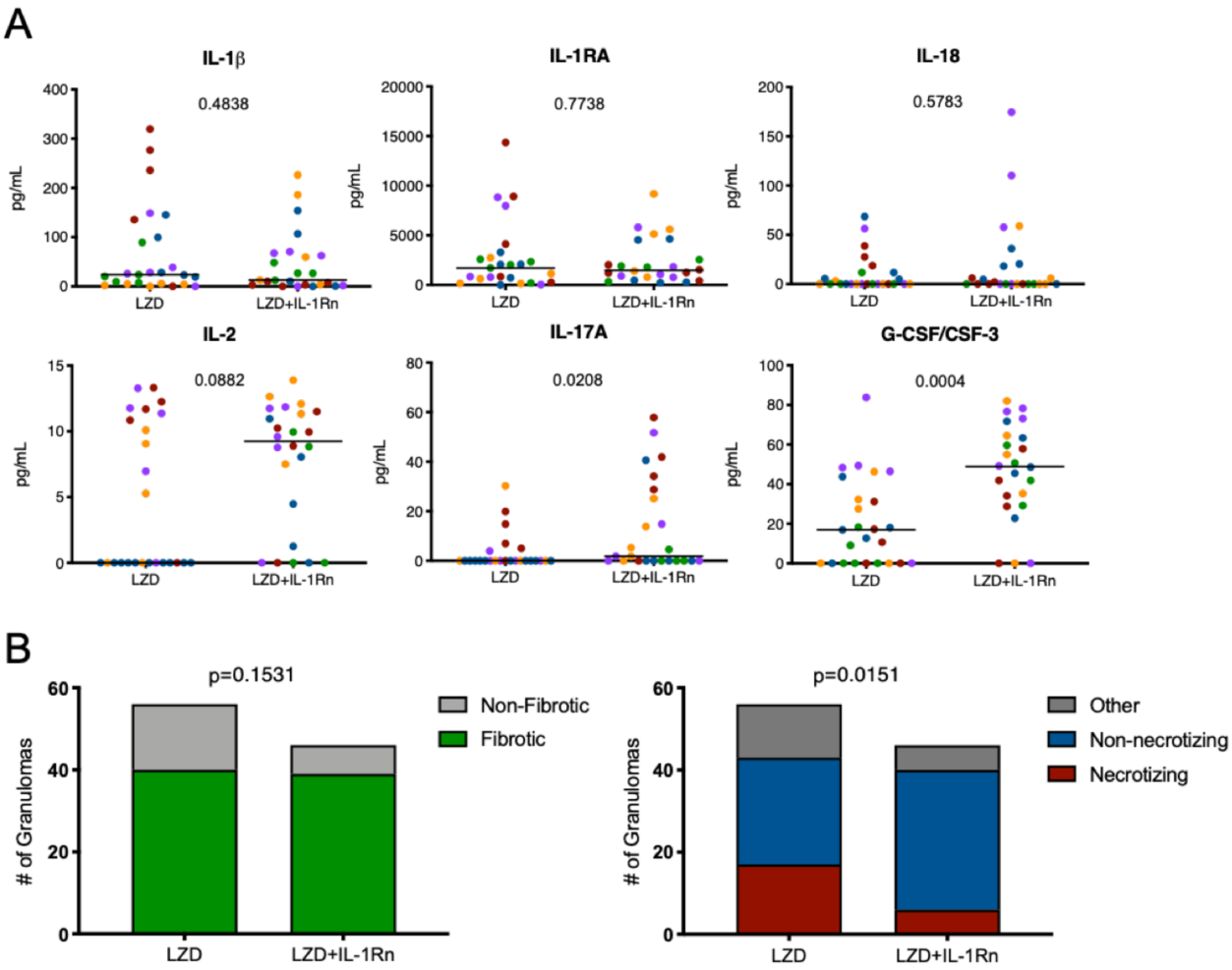

Treatment	% Fibrotic	% Non-necrotizing	% Necrotizing
LZD	71.43	46.43	30.36
LZD+IL1-Rn	84.78	73.91	13.04

Figure 8. Inflammation modulation by HDT influences granuloma resolution

Randomly selected granulomas (n=5 per macaque, n=25 per treatment group) were subjected to multiplex analysis to determine differences between treatment groups (colors indicate lesions from a single animal). p values shown determined by Mann-Whitney test. (B) Granulomas from LZD (n=57) and LZD+IL-1Rn (n=45) were examined by a pathologist (EK) and categorized. We compared fibrotic (green) vs non-fibrotic (light gray) (left) and necrotizing (red) vs non-

849 necrotizing (blue) granuloma frequencies. Frequencies represent the percentage of all

850 granulomas within treatment groups. Fisher's exact test p-values are reported.

851

852 ## Supporting information

853 **Supplementary Table 1. List of macaques for study and PET/hot values.**

854 Provided are details regarding macaques utilized for this study. DPI = days post infection.

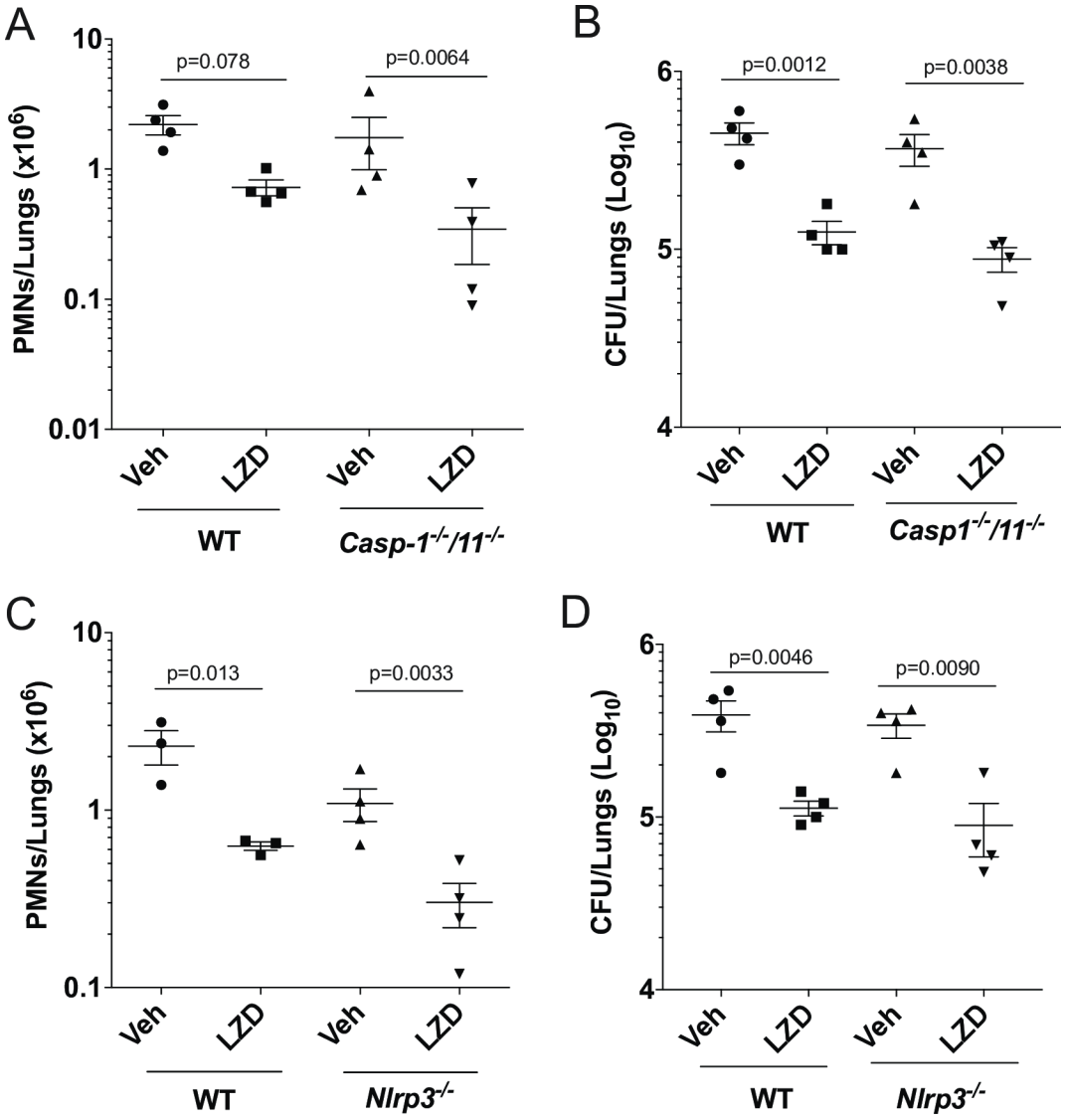

855

856 **S1 Fig. Inhibiting inflammasome signaling does not interfere with LZD efficacy.**

857 (A) Wild type C57BL/6 and *Caspase-1/11*$^{-/-}$ mice were infected with *M. tb* Erdman for 2 weeks,
858 and treated with linezolid for the subsequent 2 weeks. (A) Lung neutrophil (PMN) infiltration was
859 quantified by flow cytometry. (B) CFU in the lung are shown. Data shown (Mean ± SD) are
860 representative of two independent experiments. (C) WT and *Nlrp3*$^{-/-}$ mice were infected with *M.*
861 *tb* Erdman for 2 weeks and treated with linezolid for the following two weeks. (C) Lung
862 neutrophils were quantified by flow cytometry. (D) Bacterial burden in the lung were quantified
863 as CFU. Data shown (Mean ± SD) are from one experiment. One-way ANOVA with Sidak's
864 multiple comparison test was used to calculate the indicated p-values. N=3-5 mice used for
865 each treatment group.
866

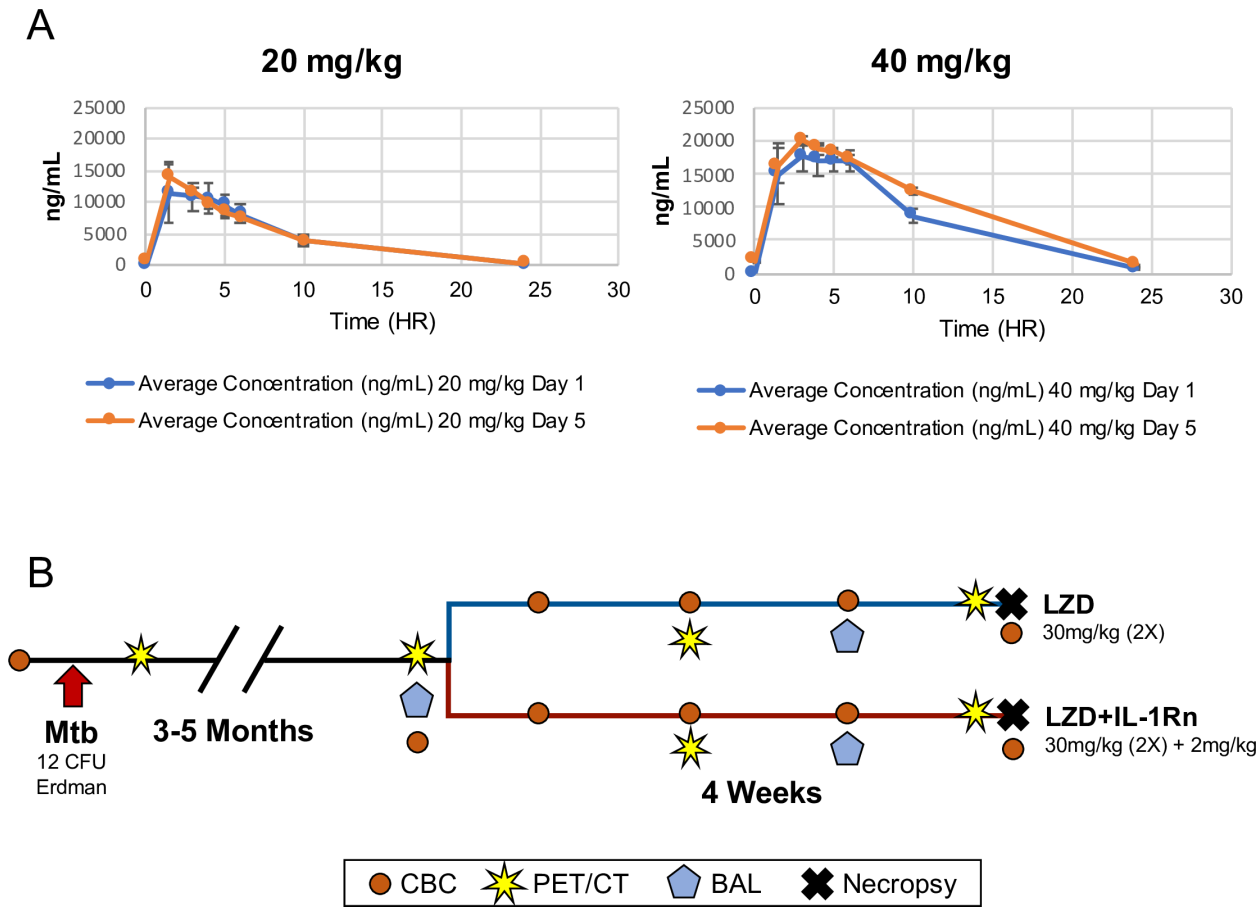

867

868 **S2 Fig. Linezolid pharmacokinetic analyses and Experimental plan for HDT in macaques**

869 (A) Plasma concentration time profiles of cynomolgus macaques receiving 20mg/kg or 40mg/kg

870 linezolid. Average plasma concentrations were plotted on Day 1 and Day 5 post-dose (n=3) (B)

871 Experimental timeline of macaque study.

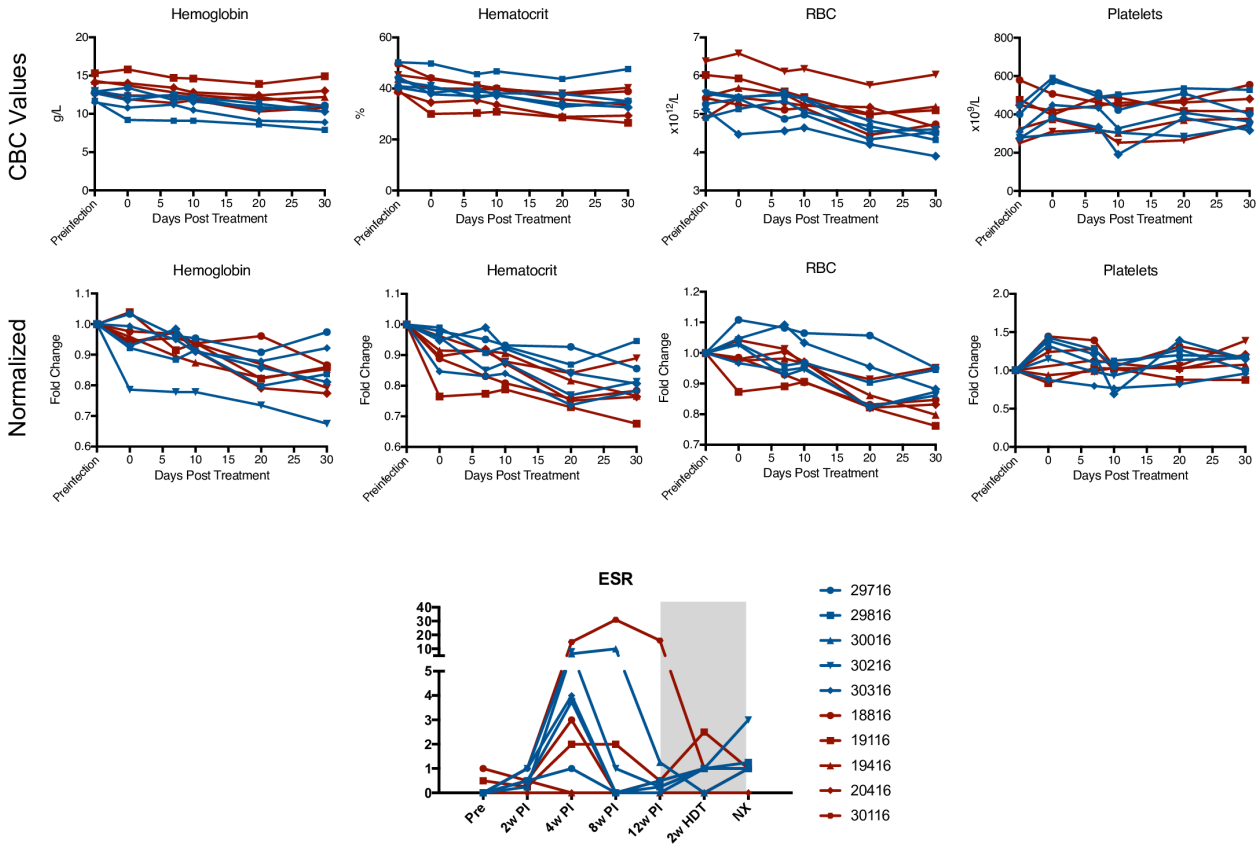

872

873 **S3 Fig. Complete blood counts and erythrocyte sedimentation rate for macaques**

874 **undergoing HDT**

875 Complete blood counts (CBCs) were taken through the study to assess anemia caused by

876 linezolid or Mtb infection. The CBC values (top) show true values for each macaque in LZD

877 (blue) or LZD+IL-1Rn (red) treatment groups. Due to variability in animal size and age, we

878 normalized CBC values to the preinfection time point for each animal (middle graphs). These

879 data indicate the relative change over the course of HDT. ESR (bottom) is a non-specific

880 measure of inflammation, LZD (blue) and LZD+IL-1Rn (red) treated macaques are depicted.

881